Global Biogeochemical Cycles®

RESEARCH ARTICLE
10.1029/2021GB007261

Large Methane Emission Fluxes Observed From Tropical Wetlands in Zambia

Jacob T. Shaw[1], Grant Allen[1], Patrick Barker[1], Joseph R. Pitt[1,2], Dominika Pasternak[3], Stéphane J.-B. Bauguitte[4], James Lee[3,5], Keith N. Bower[1], Michael C. Daly[6], Mark F. Lunt[7], Anita L. Ganesan[8], Adam R. Vaughan[3], Francis Chibesakunda[9], Musa Lambakasa[9], Rebecca E. Fisher[10], James L. France[10,11,12], David Lowry[10], Paul I. Palmer[7,13], Stefan Metzger[14,15], Robert J. Parker[16,17], Nicola Gedney[18], Prudence Bateson[1], Michelle Cain[19,20], Alba Lorente[21], Tobias Borsdorff[21], and Euan G. Nisbet[10]

[1]Centre for Atmospheric Science, Department of Earth and Environmental Science, University of Manchester, Manchester, UK, [2]Now at School of Chemistry, University of Bristol, Bristol, UK, [3]Wolfson Atmospheric Chemistry Laboratories, Department of Chemistry, University of York, York, UK, [4]Facility for Airborne Atmospheric Measurements FAAM 125, Cranfield University, Cranfield, UK, [5]National Centre for Atmospheric Science, University of York, York, UK, [6]Department of Earth Sciences, University of Oxford, Oxford, UK, [7]School of GeoSciences, University of Edinburgh, Edinburgh, UK, [8]School of Geographical Sciences, University of Bristol, Bristol, UK, [9]Geological Survey of Zambia, Ministry of Mines and Mineral Development, Lusaka, Zambia, [10]Department of Earth Sciences, Royal Holloway, University of London, Surrey, UK, [11]British Antarctic Survey, Natural Environment Research Council, Cambridge, UK, [12]Now at Environmental Defense Fund, London, UK, [13]National Centre for Earth Observation, University of Edinburgh, Edinburgh, UK, [14]Battelle, National Ecological Observatory Network, Boulder, CO, USA, [15]Department of Atmospheric and Oceanic Sciences, University of Wisconsin-Madison, Madison, WI, USA, [16]National Centre for Earth Observation, University of Leicester, Leicester, UK, [17]Earth Observation Science, School of Physics and Astronomy, University of Leicester, Leicester, UK, [18]Met Office Hadley Centre, Joint Centre for Hydrometeorological Research, Crowmarsh Gifford, UK, [19]Environmental Change Institute, School of Geography and the Environment, University of Oxford, Oxford, UK, [20]Now at Centre for Environment and Agricultural Informatics, Cranfield University, Cranfield, UK, [21]SRON Netherlands Institute for Space Research, Utrecht, Netherlands

Abstract Methane (CH_4) is a potent greenhouse gas with a warming potential 84 times that of carbon dioxide (CO_2) over a 20-year period. Atmospheric CH_4 concentrations have been rising since the nineteenth century but the cause of large increases post-2007 is disputed. Tropical wetlands are thought to account for ~20% of global CH_4 emissions, but African tropical wetlands are understudied and their contribution is uncertain. In this work, we use the first airborne measurements of CH_4 sampled over three wetland areas in Zambia to derive emission fluxes. Three independent approaches to flux quantification from airborne measurements were used: Airborne mass balance, airborne eddy-covariance, and an atmospheric inversion. Measured emissions (ranging from 5 to 28 mg m^{-2} hr^{-1}) were found to be an order of magnitude greater than those simulated by land surface models (ranging from 0.6 to 3.9 mg m^{-2} hr^{-1}), suggesting much greater emissions from tropical wetlands than currently accounted for. The prevalence of such underestimated CH_4 sources may necessitate additional reductions in anthropogenic greenhouse gas emissions to keep global warming below a threshold of 2°C above preindustrial levels.

Plain Language Summary Methane (CH_4) is a powerful greenhouse gas. The more CH_4 in the atmosphere, the greater the amount of warming. CH_4 is emitted naturally by many sources, such as wetlands, but is also emitted by many human activities, such as fossil fuel use, waste treatment, and farming. Tropical wetlands are thought to account for roughly one-fifth of the global CH_4 emissions, but studies on tropical wetlands in Africa are extremely rare. We measured CH_4 emissions from three separate wetlands in Zambia (southern Africa) and found that models were estimating much lower CH_4 emissions. If more CH_4 is being emitted by the many other African wetlands than currently thought, then we may have overestimated the amount of CH_4 that humans can yet emit before reaching 2°C of global warming, and failing the promises set out in the Paris Agreement.

Key Points:

- Quantification of the first methane emission fluxes from Zambian wetlands using world-first airborne survey data recorded over Zambia
- Intercomparison of, and guidance on, the use of three independent approaches for flux quantification from aircraft surveys
- Wetland methane fluxes were observed to be significantly greater than those simulated by Global Carbon Project land surface models

Supporting Information:

Supporting Information may be found in the online version of this article.

Correspondence to:

J. T. Shaw, G. Allen and E. G. Nisbet, jacob.shaw@manchester.ac.uk; grant.allen@manchester.ac.uk; E.Nisbet@rhul.ac.uk

Citation:

Shaw, J. T., Allen, G., Barker, P., Pitt, J. R., Pasternak, D., Bauguitte, S. J.-B., et al. (2022). Large methane emission fluxes observed from tropical wetlands in Zambia. *Global Biogeochemical Cycles*, *36*, e2021GB007261. https://doi.org/10.1029/2021GB007261

Received 26 NOV 2021
Accepted 20 MAY 2022

Author Contributions:

Conceptualization: Grant Allen, James Lee, Paul I. Palmer, Michelle Cain, Euan G. Nisbet
Data curation: Jacob T. Shaw, Patrick Barker, Joseph R. Pitt, Stéphane J.-B. Bauguitte, Mark F. Lunt, Rebecca E. Fisher, James L. France, Robert J. Parker, Prudence Bateson
Formal analysis: Jacob T. Shaw, Joseph R. Pitt, Dominika Pasternak, Mark F. Lunt, Anita L. Ganesan, Adam R. Vaughan, Rebecca E. Fisher, James L. France

Funding acquisition: Grant Allen, James Lee, Anita L. Ganesan, Paul I. Palmer, Euan G. Nisbet
Investigation: Grant Allen, Patrick Barker, Joseph R. Pitt, Stéphane J.-B. Bauguitte, James Lee, Keith N. Bower, Michael C. Daly, Rebecca E. Fisher, James L. France, David Lowry, Prudence Bateson
Methodology: Jacob T. Shaw, Grant Allen, Joseph R. Pitt, Dominika Pasternak, James Lee, Mark F. Lunt, Anita L. Ganesan, Adam R. Vaughan, Rebecca E. Fisher, James L. France, David Lowry, Paul I. Palmer, Stefan Metzger, Robert J. Parker, Prudence Bateson
Project Administration: Grant Allen, Stéphane J.-B. Bauguitte, James Lee, Keith N. Bower, Euan G. Nisbet
Resources: Francis Chibesakunda, Musa Lambakasa, Alba Lorente, Tobias Borsdorff
Supervision: Grant Allen, James Lee, Paul I. Palmer, Euan G. Nisbet
Visualization: Jacob T. Shaw, Dominika Pasternak, Michael C. Daly, Mark F. Lunt, Anita L. Ganesan, James L. France
Writing – original draft: Jacob T. Shaw, Grant Allen, Joseph R. Pitt, Dominika Pasternak, Michael C. Daly, Mark F. Lunt, Anita L. Ganesan, James L. France, Paul I. Palmer, Euan G. Nisbet
Writing – review & editing: Jacob T. Shaw, Grant Allen, Joseph R. Pitt, Dominika Pasternak, James Lee, Michael C. Daly, Mark F. Lunt, Anita L. Ganesan, Adam R. Vaughan, Rebecca E. Fisher, James L. France, David Lowry, Paul I. Palmer, Robert J. Parker, Euan G. Nisbet

1. Introduction

Following a period of stabilization between 1999 and 2006, atmospheric methane (CH_4) concentrations have exhibited largely unexplained and accelerating growth (Dlugokencky, 2020). This growth was accompanied by a switch in the long-term trend in the carbon isotopic ratio of CH_4 (expressed as $\delta^{13}C_{CH_4}$) (Lan et al., 2021; Nisbet et al., 2016, 2019): prior to 2006, the bulk global isotopic signature had been shifting toward more positive values of $\delta^{13}C$. However, the trend since 2007 has become increasingly negative, as a result of isotopically lighter global atmospheric CH_4 (Nisbet et al., 2019). Such a shift in the isotopic trend implies a significant rebalancing of CH_4 sources and sinks. Possible explanations for these observations include increasing fossil fuel emissions (Howarth, 2019; Milkov et al., 2020; Schwietzke et al., 2016), increasing biogenic emissions (Lunt et al., 2019; Schaefer et al., 2016; Wilson et al., 2021), or declining CH_4 removal by atmospheric oxidants (McNorton et al., 2018; Rigby et al., 2017). Taken individually, such explanations cannot fully reconcile both the increase in CH_4 and the isotopic shift, suggesting that the true explanation is more likely a combination of all these factors (Jackson et al., 2020; Nisbet et al., 2019).

According to recent bottom-up and top-down inventories, emissions of CH_4 from tropical wetlands account for approximately 20% of the total global source (Saunois et al., 2020), and are thought to dominate the interannual variability in global CH_4 growth (Parker et al., 2018). Despite this, emissions of CH_4 from tropical wetlands are extremely poorly quantified, both in terms of their magnitude and their isotopic signature (Ganesan et al., 2019). This is especially true for tropical wetlands in Africa, representing a substantial geographical gap in our knowledge of the global CH_4 budget (Ganesan et al., 2019; Kim et al., 2016). Seasonal CH_4 fluxes of between 5 and 25 mg m-2 hr-1 have recently been reported for a permanent wetland in the Okavanga Delta, Botswana (Helfter et al., 2021, 2022) but these remain some of the only CH_4 flux measurements available for wetlands in tropical Africa. Although statistically consistent within their estimated uncertainty ranges, there is a ~30 Tg yr^{-1} mismatch between mean bottom-up and top-down estimates of global wetland CH_4 emissions, with top-down estimates generally reported to be larger than bottom-up estimates implying a possible underestimation by land surface models (Saunois et al., 2020).

Where measurements of CH_4 emissions from tropical wetlands do exist, they have typically relied on surface emission samples collected using flux chambers, and analyzed offline using gas chromatography (e.g., Marani & Alvalá, 2007; Nahlik & Mitsch, 2011). Such surface chamber measurements potentially miss important vectors for emission, in which vegetation may function as a conduit (Barba et al., 2018; Pangala et al., 2017). African vegetated marshland ecosystems are typically dominated by tall papyrus and phragmites, which may vent CH_4 directly to the atmosphere above the vertical capture range of most surface flux measurement chambers (Barba et al., 2018; Pangala et al., 2017). Long-term research stations with instrumented towers can be used to measure fluxes above the vegetation canopy (e.g., Dalmagro et al., 2019; Helfter et al., 2021), but their prevalence in tropical wetland environments is limited, particularly in Africa.

Land surface models simulate wetland CH_4 fluxes via a series of production, oxidation, and transportation processes, computed as the product of an emission flux density and the surface spatiotemporal wetland extent (Melton et al., 2013; Saunois et al., 2020). These models are typically used in global budgets to provide bottom-up estimates of wetland emissions. However, many land surface models do not explicitly model vegetation type or density, and have been reported to inaccurately diagnose vegetated marshland areal extent (Blyth et al., 2021; Melton et al., 2013). The lack of observational CH_4 emission data means that many land surface models are poorly parameterized and poorly constrained for tropical wetlands (Parker, Wilson, et al., 2020). Models are therefore unable to simulate emissions accurately across heterogeneous land types and timescales (Lan et al., 2021; Wilson et al., 2021; Xu et al., 2016). There is also growing evidence that climatic feedback may lead to increased CH_4 emission from natural sources (including tropical wetlands) driven by increasing rainfall and rising temperatures (Dean et al., 2018; Lunt et al., 2021; Nisbet et al., 2019). Highly uncertain and positive climate feedback from natural systems may necessitate further reduction measures on anthropogenic greenhouse gas emissions than those currently modeled and planned for, to keep global warming below a threshold of 2°C above preindustrial levels (Comyn-Platt et al., 2018).

Recently, satellites have observed high CH_4 concentrations over tropical East Africa, corresponding to higher-than-expected emissions from wetlands, which were estimated to be up to an order of magnitude greater than emissions simulated by land surface models (Lunt et al., 2019, 2021; Pandey et al., 2021). However, satellite

measurements of CH_4 are typically limited to cloud-free conditions (Palmer et al., 2021). While satellites can observe the influence of substantial emissions at large distances downwind of a source (particularly important when there is widespread cloud cover over the source region of interest), aircraft-based measurement platforms offer focused sampling in all conditions, at a higher spatial resolution, and in closer proximity to the source.

A variety of approaches can be used to estimate surface emission fluxes from airborne measurements, each of which involves some model of atmospheric transport and dispersion. Airborne mass balance box modeling techniques have been extensively used to quantify fluxes from disperse regional sources such as wetlands, cities, and industrial areas (e.g., Fiehn et al., 2020; O'Shea et al., 2014; Pitt et al., 2019). Advective mass balance models assume horizontal transport with the mean wind vector, and limited exchange between the planetary boundary layer (PBL) and the free troposphere (Pitt et al., 2019). Advective mass balance models typically require capturing the full extent of an emission plume downwind of a source by flying transects at multiple altitudes, but results can be severely impacted by significant boundary layer development (Cambaliza et al., 2014). Boundary layer budgeting mass balance models are based on the rate of change of a gas within a well-mixed volume, and can account for rapid boundary layer development but with limited horizontal transport (Denmead et al., 1999). The airborne eddy-covariance approach is an emerging technique which provides spatially resolved flux measurements that are especially useful for heterogeneous sources. However, eddy-covariance measurements require expensive, high time-resolution instrumentation with parallel sampling of three-dimensional winds, and is highly dependent on meteorology (e.g., Hannun et al., 2020; Metzger et al., 2013; Vaughan et al., 2016, 2021). Finally, atmospheric inversion modeling is driven by numerical weather prediction models and thus can account for spatial and temporal variability in meteorological conditions (Ganesan et al., 2014, 2017; Rigby et al., 2019). Inversion modeling usually utilizes long-term, ground-based measurements to estimate surface fluxes on regional or global scales, but has been successfully applied to relatively short time-scale aircraft measurements (Brioude et al., 2013; Lopez-Coto et al., 2020; Pisso et al., 2019). Inversion approaches can be computationally expensive to run and can also be constrained by the magnitude and spatial distribution of prior flux estimates, which may be of limited accuracy in tropical Africa. Consequently, there is no single best practice approach to aircraft-based flux quantification that works in all circumstances, and methods must often be adapted to specific survey conditions.

Here, we have measured emissions of CH_4 from previously unstudied tropical wetlands in the Congo and Zambezi drainage basins of the Central African Plateau (Daly et al., 2020). Using airborne measurements over three wetland regions in Zambia, and the three flux techniques described above, we have calculated CH_4 emission fluxes that are an order of magnitude larger than those simulated by land surface models. This may imply that CH_4 production and emission processes for the types of vegetation typical of African wetlands are not accurately represented in models. Direct measurements of CH_4 emissions from tropical wetlands are urgently required to improve the predictive capacity of land surface models, and to help balance bottom-up and top-down estimates of the global budget. We discuss this in the following sections through comparisons of our measured fluxes with both satellite and land surface model data sets.

2. Materials and Methods

Airborne measurements of CH_4 were recorded over Zambia in February 2019 as part of the Methane Observations and Yearly Assessments (MOYA; Barker et al., 2020; Wu et al., 2021) ZWAMPS field campaign. Three wetland areas were targeted across three separate flights; the Bangweulu wetland region in north-eastern Zambia (11°36' S, 30°05' E), the Kafue wetland in southern Zambia (15°43' S, 27°17' E), and the Lukanga wetland in central Zambia (14°29' S, 27°47' E) (Figure 1). These three wetlands are among the largest wetland regions in Zambia, but were also those within easy access of Lusaka Airport. Together, the three wetlands are representative of the types of wetland environments in Zambia and central Africa. The UK Facility for Airborne Atmospheric Measurements (FAAM; https://www.faam.ac.uk/) BAe-146 atmospheric research aircraft performed the flight surveys reported here.

2.1. Sampling Regions and Local Meteorology

The Bangweulu wetland region is an extensive wetland ecosystem in the Upper Congo drainage basin (Daly et al., 2020) comprising Lake Bangweulu, marshlands, floodplains, and multiple small bodies of shallow water

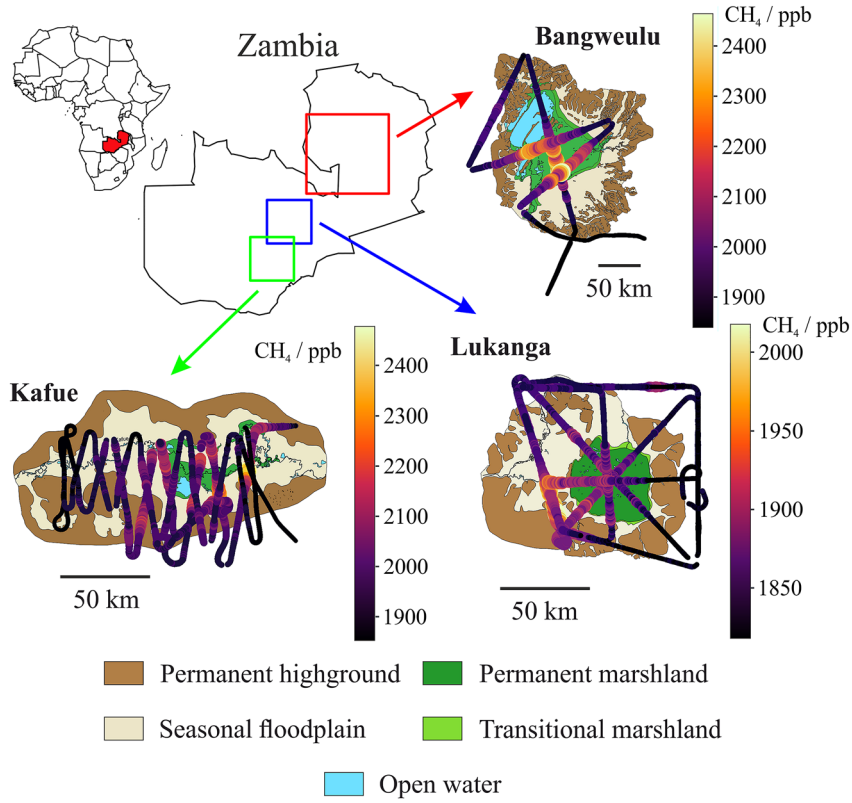

Figure 1. Methane (CH_4) mole fraction measurements over the three wetlands. Flight tracks for the flights surveying the Bangweulu (top right; 1 February 2019, 11:30:00–13:30:00 LT), Kafue (bottom left; 2 February 2019, 09:00:00–12:30:00 LT), and Lukanga (bottom right; 3 February 2019, 10:00:00–13:00:00 LT) wetlands, and their respective locations within Zambia (top left). Flight tracks are colored by CH_4 mole fraction (see scale bars). Ecosystem maps were constructed on the basis of mapping by The Ecological Survey of Zambia (Smith, 2001), and Debenham (1952), combined with field observations and Landsat satellite image interpretations. The ecosystems are defined as open water, permanent and transitional papyrus marshland, seasonally flooding grasslands, and high-ground Combretum woodland that surrounds and defines the wetland areas. The greatest CH_4 enhancements were measured over, and downwind of, vegetated marshland. See Figure S2 in Supporting Information S1 for alternative maps overlaid over satellite images. Time series of these data are also shown in Figure 4.

(Hughes & Hughes, 1992). The combined area of the lake and wetlands can reach approximately 11,000 km^2, with the permanent open water surface of Lake Bangweulu accounting for approximately 3,000 km^2 of this (Information Sheet on Ramsar Wetlands, 2007b; Travaglia & Macintosh, 1997). The Bangweulu wetland region was surveyed during the wet season, on the morning of 1 February 2019 (11:30:00–13:00:00 LT). The flight surveyed a large area over the wetland but at only a single altitude (~1600 masl) owing to the size of the survey area, the distance from the airport of origin, and limited flight duration (see Supplementary Information Table S1 in Supporting Information S1).

The Kafue wetland is an expansive, seasonally inundated floodplain around the Kafue River (Information Sheet on Ramsar Wetlands, 2007a; Hughes & Hughes, 1992). The wetlands are approximately 250 km long, and may be up to 60 km wide during floods, establishing a wetland area of approximately 6,600 km^2. Dams at either end of the Kafue River regulate the flow of water. The area was surveyed on the morning of 2 February 2019 (09:00:00–12:30:00 LT) with the intention of measuring CH_4 emission fluxes from different parts of the Kafue wetland by crossing over the river system at various points.

The Lukanga wetland occupies a shallow depression in the center of Zambia within the Zambezi drainage basin (Hughes & Hughes, 1992; Information Sheet on Ramsar Wetlands, 2005). The permanent marshland is roughly circular, with an area of approximately 1,850 km^2. There are an additional 750 km^2 of wetted regions around the surrounding river systems. The Lukanga wetland was surveyed during the morning of 3 February 2019

(10:00:00–13:00:00 LT). The smaller extent of Lukanga meant that multiple stacked transects at different altitudes were flown during both the upwind and downwind legs.

Zambian meteorology between December and March is modulated by the northward progression of the Intertropical Convergence Zone. The weather in northern Zambia during February is characterized by heavy rain and daily thunderstorms, thus requiring a localized treatment of the mixing and dilution processes necessary for emission flux quantification.

2.2. Instrumentation

A range of instrumentation for the observation of chemical and meteorological parameters was deployed on the FAAM BAe-146 aircraft. Here we describe only those measurements pertinent to this study.

The FAAM aircraft core instrument suite measured meteorological and thermodynamic parameters: air temperature was recorded by a Rosemount 102 Total Air Temperature probe (estimated uncertainty ±0.1 K); static pressure was measured by a series of pitot tubes mounted across the aircraft skin (uncertainty ±0.5 hPa); and three-dimensional wind components were measured by a nose-mounted five-port turbulence probe (uncertainty ±0.5 m s^{-1}).

A Fast Greenhouse Gas Analyzer (FGGA; Los Gatos Research Inc.; O'Shea et al., 2013) measured CH_4 mole fraction. The FGGA was calibrated in-flight using calibration gases traceable to the World Meteorological Organization (WMO) greenhouse gas scale (WMO-CH4-X2004A). The total derived uncertainty (1σ), which accounts for uncertainties in calibration and in water vapor correction, was ±2.93 ppb for the 10 Hz calibrated dry CH_4 mole fraction data (see O'Shea et al., 2013 for more details). The instrument precision was 2.11 ppb at 10 Hz, and 0.63 ppb at 1 Hz. While data were acquired at 10 Hz, the true time resolution of the instrument was closer to 6 Hz due to restricted cell flushing rates. 6 Hz measurements were achieved using an additional pump (Edward's nXDs 20i) and by adjusting the cavity pressure to 140 Torr, relative to the 1 Hz instrument setup described by O'Shea et al. (2013).

$\delta^{13}C_{CH_4}$ was measured from whole air samples collected using a manually triggered system onboard the FAAM aircraft (Fisher et al., 2017). Samples of both background and enhanced CH_4 were collected to capture a range in mole fractions. Mole fractions were measured in the RHUL laboratory using a Picarro 1301 cavity ring-down spectrometer (precision = ±0.3 ppb) calibrated using gases traceable to the WMO greenhouse gas scale (WMO-CH4-X2004A). Isotopic analysis was carried out using continuous-flow gas chromatography coupled to isotope-ratio mass spectrometry (precision = ±0.05‰; Fisher et al., 2006).

2.3. Flux Quantification

2.3.1. Airborne Mass Balance

Mass budget, or mass balance, approaches have been used to derive regional-scale fluxes of trace gases from airborne measurements (e.g., Cambaliza et al., 2014; Denmead et al., 1996, 1999; Fiehn et al., 2020; O'Shea et al., 2014; Pitt et al., 2019). There are different approaches to mass balance flux quantification, based on differing assumptions regarding boundary layer meteorology (Denmead et al., 1999). One approach is to consider the net mass flux into a column of air advected horizontally by the mean wind field (in the Lagrangian frame), bounded by the surface at the bottom, and by the PBL height at the top. The surface flux can be calculated by considering the change in concentration within the column and the net flux through the upper bound of the column (Denmead et al., 1996), as in Equation 1:

$$F_{CH_4} = h\frac{dCH_4}{dt} - (CH_4{}^{+} - CH_4)\left(\frac{dh}{dt} - W^{+}\right) \quad (1)$$

Here, F_{CH_4} is the scalar flux density of CH_4 at the surface, h is the height of the PBL above the ground, CH_4 is the CH_4 concentration within the PBL, $CH_4{}^{+}$ is the CH_4 concentration just above the PBL, and W^{+} is the vertical wind speed just above the PBL.

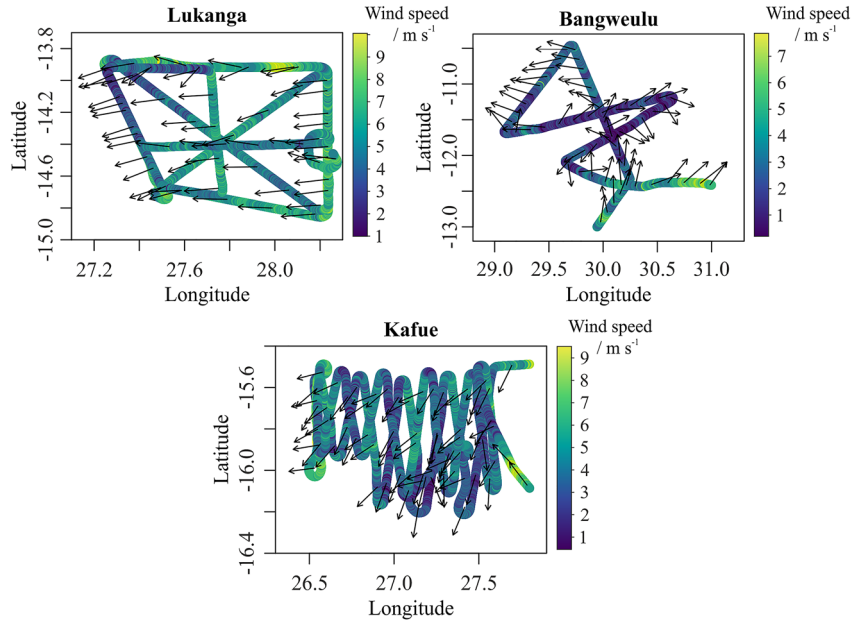

Figure 2. Wind field measurements over the three wetlands. Flight tracks for the flights sampling the Lukanga (top left), Bangweulu (top right), and Kafue (bottom) wetlands, colored by wind speed (m s^{-1}). The black arrows indicate the mean wind direction measured at 180 s intervals (Lukanga and Kafue), or 90 s intervals (Bangweulu). The wind direction was highly variable over the Bangweulu wetland but generally northeasterly over the Kafue and Lukanga wetlands. Mean wind speeds were 2.7 (±1.5), 4.2 (±1.6), and 5.6 (±1.7) m s^{-1} during the Bangweulu, Kafue, and Lukanga survey, respectively. Time series of these data are also shown in Figure 4.

Alternatively, surface flux can be measured by integrating an emission plume across a vertical plane measured downwind of a source, as in Equation 2 (e.g., Cambaliza et al., 2014; Fiehn et al., 2020; O'Shea et al., 2014; Pitt et al., 2019). The background CH_4 concentration can be taken from either the free troposphere or the upwind measurements (the difference between the free tropospheric concentration and upwind boundary layer concentrations was observed to be small in this study).

$$E_{CH_4} = h_{dw} \int_a^b (CH_4 - CH_4^+) u_\perp dx \quad (2)$$

Here, CH_4 enhancement ($CH_4 - CH_4^+$) and the wind speed perpendicular to the vertical plane ($u_\perp$) are integrated between two points, a and b, which lie outside the lateral boundaries of the wetland emission plume. The subscript on h_{dw} is shown to indicate that PBL height was measured during the downwind transect.

We used Equation 2 to derive a bulk CH_4 flux (in kg s^{-1}) for the Lukanga wetland, as the assumption of a constant wind speed and wind direction was appropriate. For the Bangweulu wetland flight, the wind speed was exceptionally low over the wetland (<2 m s^{-1}) and the wind direction highly variable (see Figure 2), so the per-unit area emission flux (in mg m^{-2} hr^{-1}) from the wetland was calculated directly from Equation 1. The two mass balance equations are fundamentally similar under certain assumptions (see Text S2 in Supporting Information S1). While the nature of the two mass balance equations necessarily yields emission estimates with different units, conversion between the two outputs is simple, requiring only an approximation of wetland surface area. However, assessment of wetland extent is not trivial, not least because wetlands are seasonally dynamic by nature, but also due to inconsistencies in land surface classification within land cover climatologies. We used the Ramsar estimates (Information Sheet on Ramsar Wetlands, 2005, 2007a, 2007b) for each of the three wetlands but a variety of other estimates of wetland area also exist (described in Text S3 in Supporting Information S1).

Three aircraft transects were flown downwind of the Lukanga wetland, roughly perpendicular to the mean wind direction. The largest CH_4 enhancements were observed during the lowest altitude transect, and decreased with both altitude and with time (the higher altitude transects were flown at later points in the morning), owing to the development of the local convective boundary layer over time. The observed decrease in CH_4 enhancement with

increasing altitude was assumed to be a consequence of the expanding boundary layer, and thereby dilution of the PBL with entrained air from the free troposphere (where CH_4 is lower in concentration), rather than as a result of poor vertical mixing within the PBL.

2.3.2. Airborne Eddy-Covariance

Airborne eddy-covariance (AEC) gives direct quantification of vertical eddy-fluxes from aircraft (Hannun et al., 2020; Metzger et al., 2013; Vaughan et al., 2016, 2021). A vertical eddy-flux is defined as the product of the fluctuating vertical wind speed and the fluctuating concentration (of CH_4), averaged over a defined period. Measuring emission fluxes using airborne eddy covariance is highly complex, and usually requires a reasonably strong and homogeneous horizontal wind, as well as a developed PBL which allows for airborne sampling well within the entrainment zone (Metzger et al., 2012).

Flux averages at 500 m intervals for each flight transect were calculated using the eddy4R algorithm code-base. Fast (>10 Hz) meteorology, position (except for altitude at 1 Hz), and CH_4 dry mole fraction (6 Hz) data were combined, and aircraft roll angles (turns) greater than 20° filtered out. Transect lengths were kept long (>30 km), with altitude variations limited to within 10% from the mean, to ensure large-scale eddy contributions to measured fluxes were captured. Only transects below 600 magl were considered to ensure measurements were well within the PBL.

Dry CH_4 mole fractions were lag-time corrected against vertical wind speed using cross-correlations. Fluxes were calculated along each flight track using mean-detrending and a wavelet-based approach. In addition, meteorological statistics (Foken & Wichura, 1996; Vickers & Mahrt, 1997), signal-to-noise statistics (Foken & Wichura, 1996; Vickers & Mahrt, 1997), limits of detection (Billesbach, 2011), and flux uncertainties (Lenschow et al., 1994; Mann & Lenschow, 1994) were calculated. Fluxes were corrected for vertical flux divergence following a prescribed method (Deardorff, 1974; Sorbjan, 2006).

Equation 3 gives the global flux covariance ($COV_{a,b}$) between instantaneous vertical wind (x) and instantaneous concentration (y) (Metzger et al., 2013).

$$COV_{a,b} = \frac{\delta j \delta t}{c \delta N} \sum_{j=0}^{J} \sum_{n=0}^{N} \frac{w_x(a_j, b_n) w_y(a_j, b_n)^*}{a_j} \tag{3}$$

where C_δ defines the wavelet-specific reconstruction factor (Morlet wavelet = 0.776), a_j defines the exponentially spaced frequency domain scales and b_n the linearly spaced time-domain scales. δt defines the unit of increment in the time-domain and δj in the frequency domain. We used a δj value of 0.125, and a frequency scale range of 0.33 s (Nyquist frequency) to 512 s.

Fluxes with a low signal-to-noise ratio (Foken & Wichura, 1996; Vickers & Mahrt, 1997) or with the integral turbulence characteristics below 100% were omitted. Random (117.9%) and systematic (21.2%) errors were calculated for each 500 m flux measurement, accounting for short averaging periods and undersampling of the largest atmospheric scales (Lenschow et al., 1994; Mann & Lenschow, 1994). As each flux measurement is temporally limited, aggregating and averaging emission fluxes across multiple transects reduces overall uncertainty. All measured fluxes were below the boundary layer (Z_i), with an average boundary layer depth (Z_m/Z_i) of 0.42. Atmospheric stratification was found to be mostly unstable, with an average Monin-Obukhov stability parameter (Z_m/L) of −6.42.

The eddy4R algorithm was applied to each of the three wetland surveys. Unfortunately, the Bangweulu flight was unsuitable for this approach due to low wind speeds and high buildup of CH_4. This resulted in the failure of the eddy4R algorithm to find cross-correlations between instantaneous vertical wind speed and instantaneous CH_4 (or temperature), and hence a result for this wetland was not obtained (Metzger et al., 2017).

2.3.3. Atmospheric Inverse Modeling

A Lagrangian particle dispersion model, NAME (Numerical Atmospheric dispersion Modeling Environment; Jones et al., 2007), was used to simulate the relationship between surface emissions and measured CH_4 mole fraction at the aircraft sampling time and location. The relationship was quantified by releasing 10,000 inert model particles from the location of the aircraft (each minute) and tracking their movement backwards in time (for up to 30 days). Particle movement was governed by advection and random turbulence, driven by Unified Model

meteorological fields at 0.14° × 0.09° spatial, and three hourly temporal, resolution. The particles' interaction with the surface (0–40 magl) was recorded to create an atmospheric footprint for each minute of sampling. The simulation domain extended from −50° to 87° E, and from −64° to 4° N; the sensitivity to these boundary conditions was evaluated by recording the time and location at which particles left the simulation domain.

NAME has been widely used in regional inverse modeling studies (Ganesan et al., 2014, 2017; Rigby et al., 2019; Tunnicliffe et al., 2020). A hierarchical Bayesian inversion method was used to combine airborne measurements, prior emissions estimates, and the NAME atmospheric footprints (Ganesan et al., 2014). The hierarchical approach allows for model parameters (such as model transport error) to be included as hyper-parameters, as they are typically not well known a priori. 100 emission elements, four boundary condition elements, and the model error estimate were solved in the inversion. The 100 emission elements were formed by aggregating model grid cells into larger regions using a quadtree algorithm, resulting in higher resolution estimates near the aircraft sampling locations. The 100 emission elements were assumed to be independent (i.e., uncorrelated). The four boundary condition elements scaled prior boundary conditions on each horizontal edge of the simulation domain. Emissions and boundary condition parameters were governed by truncated normal probability distribution functions (PDFs). The mean PDFs were centered on prior values, with a standard deviation 15 times the mean emissions value, and 2% (approximately 30 ppb) for boundary conditions. Total observational uncertainty was calculated as the quadratic sum of measurement and model error. Measurement error was the variability in 1-min averaged data. Model errors were sampled from a uniform distribution of 0–30 ppb. The inversion was solved using Markov Chain Monte Carlo simulations with a No-U-Turn sampler for emissions and boundary conditions, and a slice sampler for the model error hyperparameter (Say et al., 2020).

Prior CH_4 emissions were formed from wetland, anthropogenic, and biomass burning sources. Wetland fraction was the mean monthly 2010–2016 values from the Surface WAter Microwave Product Series (SWAMPS; Saunois et al., 2020; Schroeder et al., 2015) at 0.5° × 0.5° resolution, updated to include wetlands under dense canopies and inland waters (Tunnicliffe et al., 2020). The wetland fraction distribution was scaled uniformly to give a total emission of 20 Tg CH_4 yr^{-1} for southern Africa, consistent with bottom-up emissions estimates from this region (Saunois et al., 2020). Anthropogenic emissions were taken from the 2012 emissions in the Emission Database for Global Atmospheric Research (EDGAR; Janssens-Maenhout et al., 2019) v4.3.2 at 0.1° × 0.1° resolution. Biomass burning emissions were the February 2019 values from the Global Fire Emissions Database (GFED; van der Werf et al., 2017) v4.1 at 0.25° × 0.25° resolution. Prior boundary conditions were the two-dimensional vertical 'curtains' on the edges of the NAME domain, taken from the 2010–2018 average mole fraction fields from the CAMS CH_4 flux inversion product v18r1 (https://ads.atmosphere.copernicus.eu/cdsapp#!/dataset/cams-global-greenhouse-gas-inversion?tab=overview). All fields were re-gridded to the model resolution used here (0.14° × 0.09°).

2.4. Land Surface Models

CH_4 flux estimates were compared with emissions estimates from two land surface model ensembles; the Global Carbon Project (GCP; Saunois et al., 2020) and WetCHARTs (Bloom et al., 2017).

The GCP data set comprises 13 land surface models run under a common protocol (Saunois et al., 2020). Wetland spatial extent was prescribed using either a remote-sensing based diagnostic wetland map (consistent between models; Zhang et al., 2021) or a prognostic wetland map (where models used their own internal approach for simulating wetland area).

WetCHARTs is a global wetland CH_4 emission model ensemble which estimates CH_4 emissions at 0.5° × 0.5° resolution (Bloom et al., 2017). Two spatial and two temporal approaches are used to determine seasonal wetland extent: spatial extent uses either the GlobCover wetlands (Bontemps et al., 2011) or the GLWD wetland extent map (Lehner & Döll, 2004); while temporal variation is simulated using either the SWAMPS satellite product (Schroeder et al., 2015) or the European Center for Medium-Range Forecasts (ECMWF) monthly ERA-Interim reanalysis data (Dee et al., 2011). There are two ensembles included within WetCHARTs version 1.0: a full ensemble comprising 324 emissions estimates, at monthly intervals for 2009–2010, and an extended ensemble containing 18 emissions estimates at monthly intervals for 2001–2015.

2.5. Regional Modeling for Satellite Comparison

Model simulations to compare different wetland emission schemes with satellite observations of CH_4 (from 2019) were carried out using a nested configuration of the GEOS-Chem (v12.6) chemistry transport model (Lunt et al., 2019; Turner et al., 2015). The model was configured using meteorological fields from the NASA Global Modeling Assimilation GEOS-FP at 0.25° × 0.3125° in a domain between −20° and 52.5° E, and −36° and 20° N, with 47 vertical levels. Lateral boundary conditions for the regional domain were generated from a 2-year global 2° × 2.5° GEOS-Chem simulation, run with prior emissions for the three main sources (anthropogenic, EDGAR v4.3.2; biomass burning, GFAS (Kaiser et al., 2012); and wetlands, WetCHARTs (Bloom et al., 2017)) and a primary sink due to CH_4 oxidation by the hydroxyl radical (giving a CH_4 lifetime of 9.9 years; Wecht et al., 2014). The GEOS-Chem global boundary condition fields were fitted to the zonal mean TROPOMI/GOSAT total column CH_4 (XCH_4) distribution, to provide pseudo-columns consistent with satellite data.

CH_4 emissions from wetlands were simulated using GEOS-Chem and the aircraft-derived emission rates from a wetland area distribution and land class adapted from the CIFOR wetlands data set (Gumbricht et al., 2017a; see Text S3 in Supporting Information S1).

2.6. Satellite Retrievals

Satellite observations (2019 only) of total column-averaged dry-air CH_4 mole fraction (XCH_4) were taken from two independent platforms: the TROPOMI instrument onboard the Sentinel 5-P satellite (Lorente et al., 2021) and the Greenhouse gases Observing SATellite (GOSAT; Butz et al., 2011; Kuze et al., 2009). TROPOMI has a swath width of 2600 km, a ground pixel of 7 × 7 km^2, and is in a sun-synchronous orbit with an overpass time of 13:30 local solar time. The bias-corrected scientific data product generated from the RemoTeC retrieval algorithm was used for this work (Butz et al., 2011; Hu et al., 2016; Lorente et al., 2021). Data were filtered for cloud coverage, surface albedo and roughness, and aerosol optical thickness. GOSAT has a ground pixel footprint of 10.5 km spaced by a 260 km across-track and 280 km along-track, and is in a sun-synchronous orbit with a local overpass time of 13:00. Quality-filtered level-2 data were taken from the University of Leicester GOSAT proxy CH_4 data set (v9.0) (Parker, Webb, et al., 2020). For comparison with the GEOS-Chem model, the TROPOMI and GOSAT data were averaged from their native resolution to a 0.25° × 0.3125° grid, consistent with the resolution of the GEOS-Chem model.

TROPOMI/GOSAT wetland enhancements were calculated using outputs from the GEOS-Chem nested model simulation. The model was sampled at the time and location of the TROPOMI/GOSAT measurements, and convolved with TROPOMI/GOSAT XCH_4 averaging kernels. The contribution of the lateral boundary conditions and the sum of all model emissions sources (except wetlands) were subtracted from the TROPOMI/GOSAT data to generate the TROPOMI/GOSAT enhancements due to exclusively wetland emissions. Emissions from anthropogenic sources (EDGAR v4.3.2; Janssens-Maenhout et al., 2019), biomass burning (GFAS; Kaiser et al., 2012), termites, and soil absorption terms were included. Livestock emissions were multiplied by a factor of 1.5 to reflect the underestimation of this emissions source in Africa in EDGAR v4.3.2 (Lunt et al., 2021).

To isolate the wetland CH_4 enhancements (from Bangweulu) from other sources, the satellite data were analyzed over a region encompassing retrievals downwind of the wetland (see Text S5 in Supporting Information S1). To do this, modeled enhancements were compared at times and locations when the GEOS-Chem wetland component from Bangweulu was greater than 5 ppb (assuming an emission rate of 21 mg m^{-2} hr^{-1}; see Results). During the 3-month period (February-April 2019), there were 115 TROPOMI and 11 GOSAT data points that met this downwind criterion. A similar analysis for the Kafue and Lukanga wetlands was not possible, as their smaller areal extent lowered the reliability of isolating wetland-dominated signals in the satellite data.

The monthly mean column enhancement over Bangweulu was also calculated for each month in 2019. To minimize the impact of other CH_4 sources, this analysis was performed over the wetland area itself (see Text S5 in Supporting Information S1). The monthly mean enhancements were used to generate a normalized seasonal cycle and multiplied by the aircraft-derived emission rate from February 2019, and the wetland extent, to generate a range of annual emissions estimates for Bangweulu.

3. Results and Discussion

Here we present measured CH_4 fluxes for three important wetland regions in Zambia (the Bangweulu, Kafue, and Lukanga wetlands). Where meteorological conditions were suitable, flux results are presented for each of the three approaches and their relative merits discussed, as advice for others attempting airborne flux calculations in varying meteorological regimes. Each method has intrinsic assumptions and limitations associated with the modeling of atmospheric transport and dispersion. Consequently, comparison of the quantified fluxes demonstrates a possible range of fluxes that can be calculated, and provides guidance on the types of conditions suitable for each method. The sampling strategy for each of the surveys was tailored to the conditions encountered, which included meteorological development over time (e.g., boundary layer development), the size of the survey region, limitations from aircraft range and flight duration, and even the presence of large flocks of birds, which may present a high flight risk.

Figure 1 shows the flight survey sampling paths over each of the three wetlands, colored by measured CH_4 mole fraction. Figure 2 shows the measured wind fields (wind direction and wind speed). Figure 3 shows the estimates of planetary boundary layer (PBL) height development over the duration of each of the three flight surveys. PBL height was inferred (by eye) from vertical profiles of potential temperature and ozone mole fraction (used as tracers of mixing and convective development) measured as the aircraft ascended or descended in altitude. Any expansion of the PBL with time, typical of tropical convection, is accounted for here in emission flux quantification using either measured or modeled (Unified Model) PBL heights. Figure 4 shows the time series of the prior and posterior estimated CH_4 mole fractions (from the atmospheric inversion approach), as a comparison with those measured during each of the flights.

In the sections below, CH_4 emission fluxes from each wetland are presented as a bulk net flux (the total emission from the entirety of the wetland area, in kg s^{-1}) and as an area-normalized flux (in mg m^{-2} hr^{-1}), where the bulk flux is normalized to the size of the wetland. Converting between these two quantities requires knowledge of the wetland area extent (see Text S3 in Supporting Information S1). Table 1 presents the CH_4 fluxes quantified for all three wetlands using the three approaches.

3.1. Methane Emission Fluxes

Figure 1 shows the measured CH_4 data superimposed over ecosystem maps of each of the three targeted wetlands. The ecosystem maps were constructed from mapping conducted by The Ecological Survey of Zambia (Smith, 2001), Debenham (1952), interpretations of Landsat satellite imagery, and in-field observations. Alternative maps, showing the CH_4 data superimposed over satellite imagery, are available in Figure S2 in Supporting Information S1. Figure 1 shows a consistent spatial association between the higher CH_4 mole fractions and areas of vegetated marshland. This was most compelling for the Bangweulu wetland but was also observed for the Lukanga wetland, with enhancements observed downwind and to the south-west of the central marshland. The association between CH_4 and vegetated marshland was least clear for the Kafue wetland, but the highest enhancements were developed downwind of the river system and associated marshland.

3.1.1. Bangweulu Wetland

Enhancements in CH_4, of up to 600 parts per billion (ppb) over the surrounding background, were measured directly above vegetated marshland in the center of the Bangweulu wetland during the flight (Figure 1). In contrast, no such enhancements were observed directly over, or nearby, large bodies of open water, such as Lake Bangweulu in the north-west of the wetland. Figure 3 shows that the PBL over Bangweulu increased in height by approximately 600 m over the 3-hr flight duration. The wind field encountered during the flight over the Bangweulu wetland was particularly variable (Figure 2), and the wind speed was generally very low over the wetland itself (<2 m s^{-1}). The lack of a clear prevailing wind direction and slow wind speed meant that enhancements were unlikely to be transported away from the emission source. These conditions were suitable for flux quantification using the boundary layer budgeting mass balance approach (Denmead et al., 1999) but were not suitable for the advective mass balance approach. Neither were the conditions suitable for analysis using the eddy-covariance technique as cross-correlations between measured vertical wind speed, temperature, and CH_4 were unable to be quantified. Hence, an emission flux for the Bangweulu wetland was quantified here using the boundary layer budgeting mass balance and the atmospheric inversion approaches.

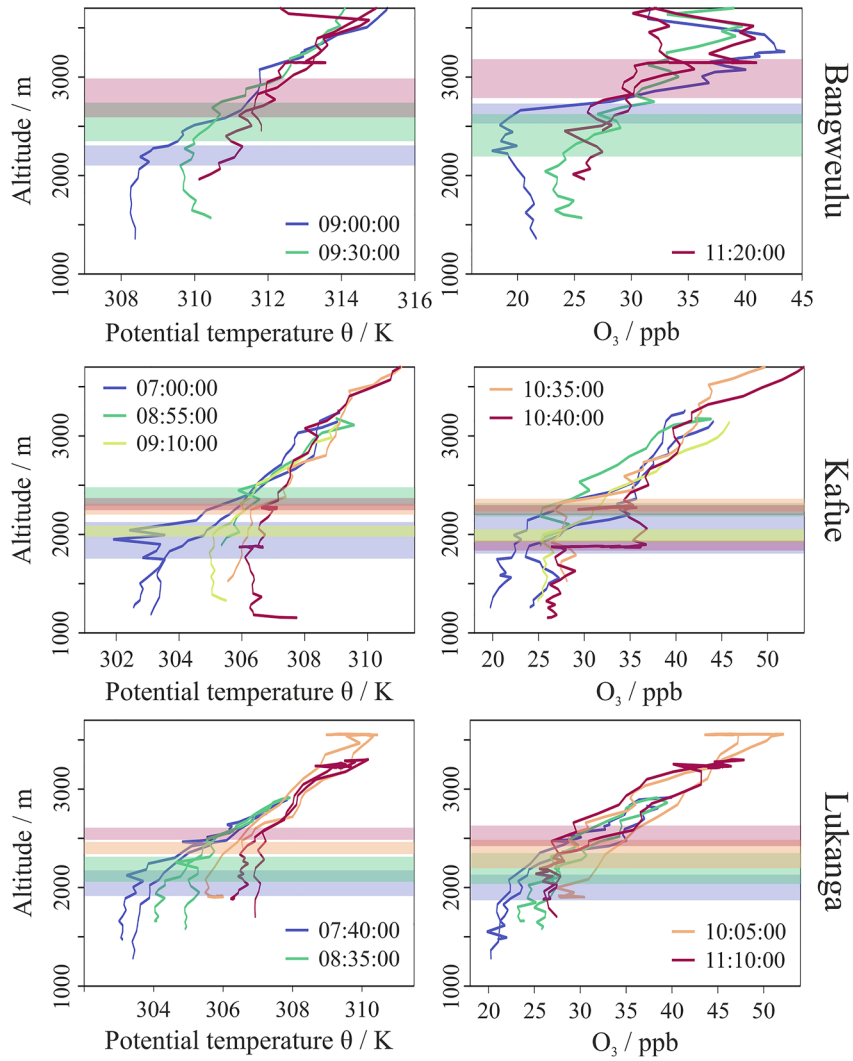

Figure 3. Estimates of planetary boundary layer (PBL) height over the three wetlands. Potential temperature (θ) and O_3 mole fraction (ppb) vertical profiles for the flights surveying the Bangweulu (top row), Kafue (center row), and Lukanga (bottom row) wetlands. Only data where the aircraft was ascending or descending in altitude is shown. The colors correspond to different time periods (UTC; LT-2) during each of the flights, with the highlighted areas indicating the uncertainty in the PBL height estimated at that time (these uncertainties were propagated through into the final emission flux uncertainty estimates). Estimates of PBL height were based on rapid or sudden changes in θ or O_3 mole fraction with altitude, or where there were substantial changes in gradient with altitude (identified by eye). The surface elevation below each of the atmospheric profiles was largely flat, with only minor elevation changes between profiles. Planetary boundary layer height increased over the course of the flights over each of the wetlands, as expected.

The boundary layer budgeting box model was used to derive an area-normalized emission flux of 21.1 (±6.1) mg CH_4 m^{-2} hr^{-1}, representing a 'snapshot' of emission fluxes for the conditions at the time of survey (Table 1). The uncertainty quoted here represents one standard deviation (1 s.d.) and was calculated through the propagation of uncertainties associated with measured wind variability (Figure 2), boundary layer mixing processes (Figure 3), and instrumental uncertainty. Accounting for the expansive extent of the Bangweulu wetland (Information Sheet on Ramsar Wetlands, 2007b), this area-normalized flux is equivalent to a bulk net emission flux of 46.9 (±13.6) kg CH_4 s^{-1}. In the atmospheric inversion approach, prior CH_4 emissions were optimized to best match measurements, yielding posterior emission fluxes from the Bangweulu wetland of 9.0 (±3.4) mg CH_4 m^{-2} hr^{-1} (Table 1). Extrapolating this result to the entire Bangweulu wetland results in a calculated bulk flux of 20.0 (±7.6) kg CH_4 s^{-1}.

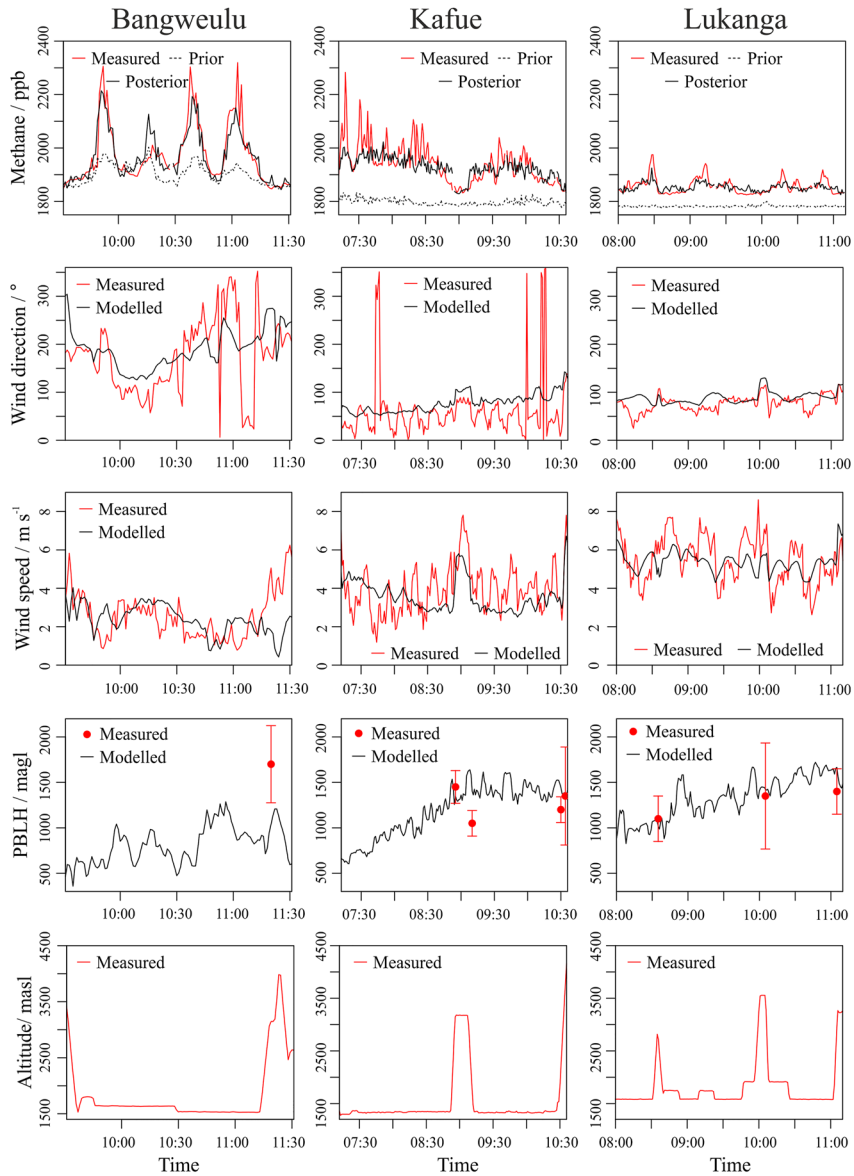

Figure 4. Time series (UTC) of measured data and simulated data used in the atmospheric inversion. Measured (red) and simulated (NAME; black) one-minute average CH_4 mole fraction, wind speed and wind direction, and empirical (see Figure 3) and simulated planetary boundary layer (PBL) heights (PLBH), for the Bangweulu (left column), Kafue (central column), and Lukanga (right column) wetland surveys. There was reasonable agreement between measured and simulated wind direction, wind speed, and PBLH, throughout all three flight surveys. Simulations performed for the NAME inversion were driven by meteorology from the Unified Model (UM), a numerical weather prediction model. The aircraft altitude (meters above sea level) during flights is also shown for additional context (see also Figure S3 in Supporting Information S1).

The CH_4 fluxes quantified for the Bangweulu wetland using the mass balance and atmospheric inversion approaches did not agree within their respective uncertainties. However, pseudo-column simulated enhancements derived using the mass balance flux were more consistent with satellite retrievals than those derived using the atmospheric inversion flux (see Section 3.3). This consistency between the mass balance method and satellite data suggests that the mass balance flux may be more accurate than that quantified using the atmospheric inversion approach. The atmospheric inversion flux may be expected to be smaller as a result of a lower PBL height used to drive the NAME transport model (using meteorology from the Unified Model) as the modeled PBL height (~1100 magl) disagreed with measurements (~1700 magl) by a factor of ~1.5 (Figure 4). We therefore

Table 1
Summary of Measured and Modeled (Month of February) Per-Unit-Area and Bulk Emission Fluxes From Each of the Bangweulu, Kafue, and Lukanga Wetlands (See Section 3.1)

	Area-normalized flux/mg m^{-2} hr^{-1}			Bulk flux/kg s^{-1}		
CH_4 emission type	Bangweulu	Kafue	Lukanga	Bangweulu	Kafue	Lukanga
Mass balance	21.1 ± 6.1	–	*15.5 ± 2.7*	*46.9 ± 13.6*	–	11.2 ± 2.0
Eddy-covariance	–	23.0 ± 31.6	27.9 ± 14.3	–	*42.2 ± 58.0*	*20.2 ± 10.3*
NAME inversion	9.0 ± 3.4	5.0 ± 0.7	14.6 ± 2.5	*20.0 ± 7.6*	*9.2 ± 1.3*	*10.5 ± 1.8*
GCP[a]	*1.7 ± 2.0*	*1.2 ± 1.6*	*3.9 ± 5.0*	3.9 ± 4.3	2.3 ± 3.0	2.8 ± 3.6
WetCHARTs[b]	*2.7 ± 2.1*	*0.6 ± 0.6*	*1.6 ± 2.3*	6.0 ± 4.7	1.2 ± 1.1	1.1 ± 1.7

Note. Values in italics represent emission fluxes calculated by conversion with the Ramsar wetland area estimates (Information Sheet on Ramsar Wetlands, 2005, 2007a, 2007b; see Text S3 in Supporting Information S1).
[a]Mean of results from 13 land surface models for the month of February, 2000–2017. [b]Mean of results from 9 land surface models in 324 different ensemble members for the month of February, 2009–2010.

provide a flux range (estimated from both approaches) for the Bangweulu wetland of 20.0–46.9 kg CH_4 s^{-1} (Table 1) using the data available for this study. Additional surveys would help to reduce this range.

3.1.2. Kafue Wetland

Widespread CH_4 enhancements of up to 300 ppb above the surrounding local background were observed over the Kafue wetland, with smaller, isolated areas of local enhancements of 600 ppb above background (Figure 1). The wind direction was generally northeasterly throughout the survey, with wind speeds of ~4 m s^{-1} (Figure 2) and the PBL demonstrated rapid growth of more than 400 m over the 4-hr flight duration (Figure 3).

A CH_4 emission flux from the Kafue wetland was quantified using the airborne eddy-covariance approach. The eddy-covariance CH_4 fluxes presented here were the first of their kind measured using this research aircraft (the FAAM BAe-146) as well as the first in tropical Africa. As such, this represents a novel advancement for CH_4 flux quantification from remote regions inaccessible to smaller aircraft with smaller flight ranges. The largest eddy-covariance fluxes (up to 150 mg CH_4 m^{-2} hr^{-1}) were measured directly over vegetated marshland (Figure 5), with a mean emission flux of 23.0 (±31.6) mg CH_4 m^{-2} hr^{-1} over the wetland area (Table 1). If the mean emission flux measured here is assumed to be representative of the average emission from the whole of the Kafue wetland, the bulk flux can be estimated to be 42.2 (±58.0) kg CH_4 s^{-1}. However, this extrapolation relies on the calculated fluxes being representative of emissions from the wider geographical region, which is difficult to determine without further study. The area-normalized flux estimate inferred from the atmospheric inversion was 5.0 (±0.7) mg CH_4 m^{-2} hr^{-1}, equivalent to a bulk flux of 9.2 (±1.3) kg CH_4 s^{-1} (Table 1). The mass balance approach was not used for the Kafue wetland despite a more consistent wind direction than that observed during the Bangweulu survey. This was due to the large and heterogeneous shape of the Kafue floodplain, and a lack of

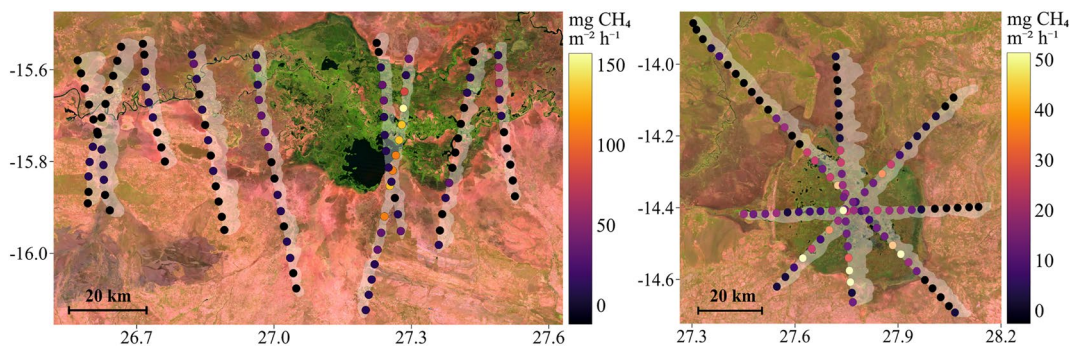

Figure 5. Airborne eddy-covariance Methane (CH_4) emission fluxes. Fluxes (mg CH_4 m^{-2} hr^{-1}) were calculated at 3 km intervals for the Kafue (left) and Lukanga (right) wetlands (see scale bar). The transparent white highlighted areas indicate the calculated emission footprints (90%). Green areas in the satellite imagery indicate wetlands. Satellite imagery © GLAD Landsat MOSAIC 2021.

representative upwind and downwind flight sampling (see Figure 1 and Figure S3 in Supporting Information S1). Mass balance methods are more suited to discrete areas with assumed homogeneous sources.

The CH_4 fluxes quantified for the Kafue wetland using the eddy-covariance and atmospheric inversion approaches agreed within their respective uncertainties, albeit with a wide range of uncertainty. The large uncertainty reported for the eddy-covariance flux was a result of high spatial variability (indicative of the heterogeneity of the sources) where significant hotspots were observed with emissions of up to 150 mg CH_4 m^{-2} hr^{-1} (Figure 5). This makes the extrapolation of a bulk net flux from a mean eddy-covariance flux problematic for highly heterogeneous environments. The meteorology used to drive the atmospheric inversion model showed good agreement with measurements of wind speed, wind direction, and PBL height for the Kafue survey (Figure 4). We therefore provide a flux range (estimated from the eddy-covariance and inversion approaches) for the Kafue wetland of 9.2–42.2 kg CH_4 s^{-1} (Table 1).

3.1.3. Lukanga Wetland

CH_4 enhancements of roughly 200 ppb over background (Figure 1) were observed to the south west of the Lukanga wetland due to a relatively strong (~6 m s^{-1}) and consistent north-easterly wind (Figure 2). Data sampled at three altitudes downwind of the Lukanga wetland permitted the use of the advective mass balance model which was used to estimate a bulk emission flux of 11.2 (±2.0) kg CH_4 s^{-1}. Using the Ramsar estimate for wetland extent (Information Sheet on Ramsar Wetlands, 2005), the area-normalized emission flux was estimated to be 15.5 (±2.7) mg CH_4 m^{-2} hr^{-1}. Eddy-covariance was used to quantify a mean emission flux of 27.9 (±14.3) mg CH_4 m^{-2} hr^{-1} (Figure 5) from the Lukanga wetland. The largest fluxes, of up to 50 mg CH_4 m^{-2} hr^{-1}, were observed over vegetated wetland regions (visible as dark green areas in the satellite imagery in Figure 5) outside of which CH_4 emissions decreased sharply (to generally <5 mg CH_4 m^{-2} hr^{-1}). The calculated emission footprint (equivalent to ~682 km^2, or ~1/4 of total wetland area) extrapolates to a bulk flux of 20.2 (±10.3) kg CH_4 s^{-1}. Finally, atmospheric inversion modeling yielded an area-normalized emission flux of 14.6 (±2.5) mg CH_4 m^{-2} hr^{-1} and a bulk flux of 10.5 (±1.8) kg CH_4 s^{-1} (Table 1).

CH_4 fluxes quantified for the Lukanga wetland using the three methods were in good agreement within their respective uncertainties. The Lukanga wetland survey presented an optimal case study for flux quantification, both in terms of the meteorological conditions during the flight and the more homogeneous nature of the emission source (Figure 5). This allowed for the application and comparison of all three flux approaches, which was not possible for Bangweulu and Kafue for the reasons described above. We provide a flux range (estimated from all three approaches) for the Lukanga wetland of 10.5–20.2 kg CH_4 s^{-1} (Table 1).

3.1.4. Comparison of Flux Quantification Approaches

This is the first study to evaluate and compare the use of mass balance, eddy-covariance, and atmospheric inversion flux quantification approaches using airborne survey data. By comparing these approaches we can offer important guidance on their applicability to future airborne surveys and survey design. Table 1 summarizes the calculated bulk and area-normalized emission fluxes for each of the approaches (where it was possible to apply them) for each wetland.

We conclude that airborne eddy-covariance analysis can be useful for examining the spatial variability of heterogeneous sources, but provides poor representation of a bulk net flux in the absence of more complete sampling than that available in this study. Strong, clear, and positive cross-correlations between vertical wind and CH_4 or temperature were used here as criteria for further analysis. Poor quality cross-correlations usually indicate unsuitable meteorological conditions, such as weak vertical transport or the highly heterogeneous wind field encountered when surveying Bangweulu.

Atmospheric inversion approaches can be useful for capturing large-scale sources that vary on spatial scales greater than the model resolution (0.14° × 0.09°), but not for sources that are highly heterogeneous in space and/or time. Atmospheric inversions attempt to account for spatial and temporal variations in meteorological conditions, such as changing PBL height or wind direction (as shown in Figure 4) that can be difficult to capture with limited field sampling. However, the inversion method relies on accuracy of those meteorological fields and thus strongly benefits from the availability of measurements to understand transport error (as shown with our Bangweulu inversion estimates). Further, atmospheric inversions may be influenced by prior emission estimates, which may be of particularly limited accuracy in tropical Africa where prior measurements are lacking.

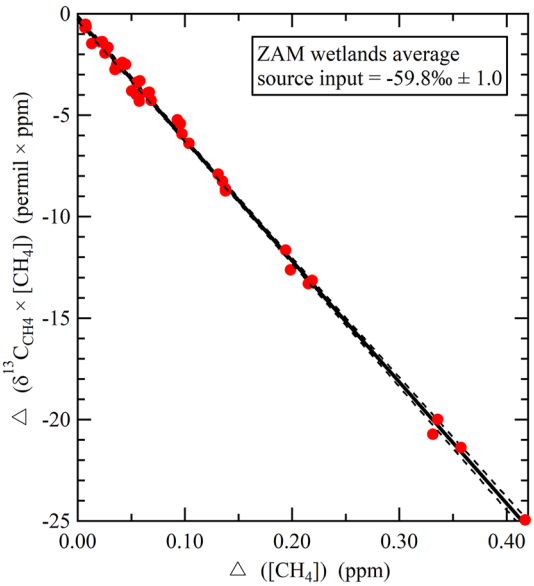

Figure 6. Methane (CH_4) isotopic signature ($\delta^{13}C_{CH_4}$) determination. Miller-Tans plot (Miller & Tans, 2003) of CH_4 sampled during flights over the three wetlands and analyzed for CH_4 carbon-isotopic signature ($\delta^{13}C_{CH_4}$). Values are plotted as differences from measured background values (i.e., $\Delta[CH_4] = [CH_4] - [CH_4]_{background}$). Thus, the Miller-Tans method accounts for non-constant background values of both $[CH_4]$ and $\delta^{13}C_{CH_4}$. The source signature is determined by the gradient of the linear regression, and is equal to −59.8‰ (±0.1.0‰.) This value is consistent with the isotopic source signatures of other tropical wetlands (Nisbet et al., 2019).

The advective mass balance approach is most suited to the evaluation of a bulk flux, but requires upwind and downwind sampling of well-mixed air masses and low variability in wind speed and direction (compared to the mean wind vector). The boundary layer budgeting mass balance method is also suited to the evaluation of a bulk flux, but only in slow (non-advective) wind conditions.

In conclusion, and by way of guidance for future aircraft flux surveys, all three approaches have utility for flux quantification, but the applied method must be carefully selected based on the survey conditions, as demonstrated by the three contrasting case studies presented in this work. In addition, repeated surveys and more complete sampling can reduce flux uncertainty.

3.2. $\delta^{13}C_{CH_4}$ Isotopic Signature

Whole air samples were collected for offline analysis of the isotopic signature of the CH_4 ($\delta^{13}C_{CH_4}$) to identify the likely emission source. Figure 6 shows a Miller-Tans plot (Miller & Tans, 2003) of sampled CH_4, demonstrating a source signature of −59.8‰ (±1.0‰). The measured isotopic signature is consistent with that reported for other tropical wetland CH_4 emissions (typically −60‰), is more enriched in ^{13}C than source signatures for temperate boreal and Arctic wetlands, and differs considerably from signatures associated with fossil fuel use (typically −45‰) (Ganesan et al., 2018; Schwietzke et al., 2016). The measured source signature may reflect the dominance of C4 plants, such as papyrus, in African wetlands. The measured global bulk signature is −47‰; thus, substantial emissions from wetlands with a source signature of −60‰ would act to drive the global CH_4 burden to more isotopically negative values. This is consistent with the observed trend in the global bulk signature post-2007 (Lan et al., 2021; Nisbet et al., 2019).

3.3. Comparisons to Satellite Observations

In this section, we compare satellite-retrieved CH_4 columns over the Bangweulu wetland with pseudo-columns simulated using the aircraft-derived CH_4 emission fluxes reported in Section 3.1, to test the validity of the calculated fluxes. Analogous satellite analyses were not performed for the Kafue and Lukanga wetlands due to a lack of satellite retrievals of column CH_4 over their smaller wetland areas, as well as their proximity to other conflating CH_4 sources.

Figure 7a shows the mean satellite-retrieved column CH_4 enhancements over, and downwind of, Bangweulu between February and April 2019 for both GOSAT (22 ± 11 ppb) and TROPOMI (19 ± 10 ppb), as well as GEOS-Chem simulated pseudo-columns. The two satellites have different CH_4 enhancement magnitudes due to differences in the spatial resolution of their retrievals, their sampling locations, and the vertical sensitivities of their instruments. The enhancements simulated using the mass balance emission rate for Bangweulu (21.1 mg CH_4 m^{-2} hr^{-1}; Table 1) were consistent with satellite observations for both GOSAT (15 ± 7 ppb) and TROPOMI (23 ± 10 ppb), which supports the magnitude of fluxes calculated using the mass balance method. However, using the lower emission rate calculated using the atmospheric inversion (9.0 mg CH_4 m^{-2} hr^{-1}; Table 1) resulted in less than half the observed enhancements for both satellites, suggesting that the inversion method underestimated true emissions in this case. The error bars (Figure 7a) reflect the uncertainty in mean column enhancements downwind of Bangweulu due to spatial variability in emissions and variations in atmospheric transport, and are similar in magnitude for retrieved and pseudo-columns. The retrievals used for this comparison were recorded after 16 February 2019, indicating the persistence of large CH_4 emissions consistent with the emission rates calculated from the aircraft data.

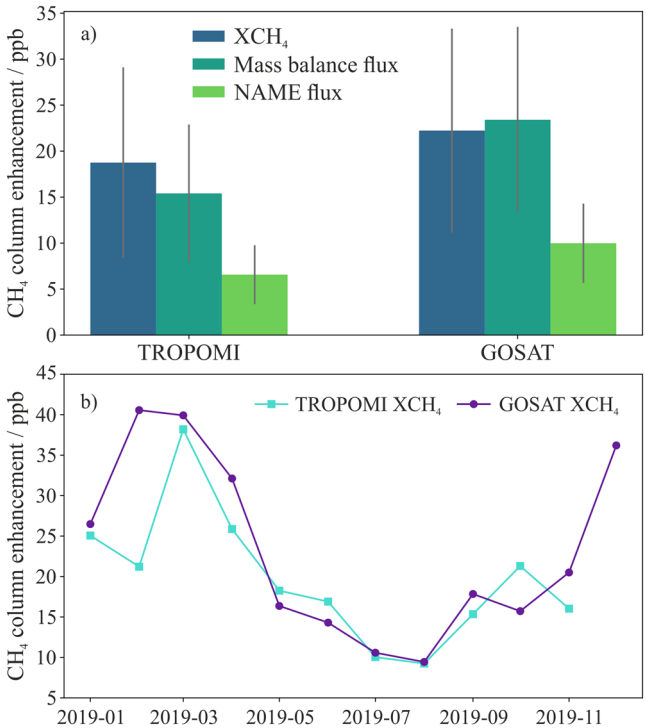

Figure 7. Total-column Methane (CH_4) (XCH_4) observations by TROPOMI and GOSAT. (a) Comparison of satellite-retrieved and pseudo-satellite XCH_4 enhancements. Satellite-retrievals (dark blue) were from TROPOMI (left) and GOSAT (right) between February and April 2019. There were no successful TROPOMI retrievals prior to 16 February 2019 due to cloud cover. Pseudo-column XCH_4 enhancements were simulated using GEOS-Chem and the two aircraft-based wetland emission fluxes calculated for Bangweulu (see Table 1). Pseudo-column enhancements using the flux calculated from the mass balance approach were in good agreement with satellite-retrievals. The error bars reflect the uncertainty in mean column enhancement downwind of Bangweulu due to spatial variability in emissions and variations in atmospheric transport. (b) TROPOMI and GOSAT retrieved monthly XHC_4 enhancements above Bangweulu for 2019. This shows the seasonality in XCH_4, with the largest enhancements occurring between December and April, and lowest between May and November.

3.4. Comparisons With Land Surface Models

Mean bulk and area-normalized CH_4 emission fluxes from the two land surface model ensembles are presented in Table 1. The models underestimated emissions by a factor of 10 on average when compared with fluxes derived from the airborne measurements (Figure 8). Examination of the 19 different wetland models used as part of the two model ensembles indicates a large inter-model variability in the magnitude and spatial distribution of CH_4 emissions (see Text S6 in Supporting Information S1). Simulated emissions were greater for the GCP models that used a diagnostic wetland area map (WAD2M (Zhang et al., 2021)), as opposed to a prognostic (internally calculated) map (Figure 8). Additionally, many of the land surface models simulated substantial emissions from model grid cells containing mostly open water, despite no clear evidence in the aircraft data for large CH_4 emissions from these areas (Figure 1): the lack of significant CH_4 enhancement over open water implied limited emissions, compared with the much stronger signals measured over surrounding vegetated wetland. Of the 19 land surface models analyzed in this study, 13 incorrectly simulated substantial emissions from model grid cells containing mostly open water, and therefore do not capture the observed dominance of vegetated wetland areas for CH_4 emissions. This could indicate that land surface models currently lack the ability to accurately predict emissions from vegetated tropical wetlands in Africa. The models may not be adequately representing important CH_4 production and emission processes for vegetation typical of African wetlands. Alternatively, the presence of vegetation may indicate regions of shallower water, and associated reduced oxidation of CH_4 between lake bed and lake surface. Regardless, improved parameterization of the main processes involved in the production of CH_4 substrate (through anaerobic muds and root exudates), and the potential vegetation-mediated transfer of CH_4 to atmosphere (where vegetation acts as a conduit) must be a priority for current and future global CH_4 budgeting, and thereby climate prediction.

3.5. Scalability

We now discuss the potential scalability of the aircraft-derived fluxes. The three surveys represent a time-limited data set, or "snapshot" of emission fluxes, particularly when viewed from an annual, or even seasonal, context. Therefore, the scalability of the calculated aircraft fluxes for periods longer than the 3 days of measurements has limited and uncertain value. Extended aircraft campaigns are expensive and labor intensive, and hence unsuitable for routine long-term monitoring. Satellites, while providing lower spatiotemporal resolution observations in cloud-free conditions, allow for continued monitoring year-round. Figure 7b shows monthly averaged XCH_4 enhancements over Bangweulu in 2019, retrieved by TROPOMI and GOSAT. An annual emission can be estimated (with important limitations) by scaling the aircraft-measured fluxes for February 2019 using the satellite column enhancements as a linear proxy for seasonality. This is a crude extrapolation as column enhancements may not necessarily correlate linearly with emissions due to seasonal variability in transport and mixing. We include the rough estimate of annual flux here to demonstrate the potential importance of Zambian wetlands in the CH_4 budget. For Bangweulu, the total annual emission was estimated to be 1.2–3.0 Tg CH_4 yr^{-1}, where the range encompasses uncertainties in the assumed wetland area (which also varies seasonally). This annual emission accounts for 4%–10% of the most recent bottom-up estimate for total African wetland emissions (30 Tg CH_4 yr^{-1}; Saunois et al., 2020), despite Bangweulu accounting for less than 1% of total sub-Saharan African wetland area (Gumbricht et al., 2017a, 2017b). However, it should be noted that interannual variations in total emissions cannot be accounted for here.

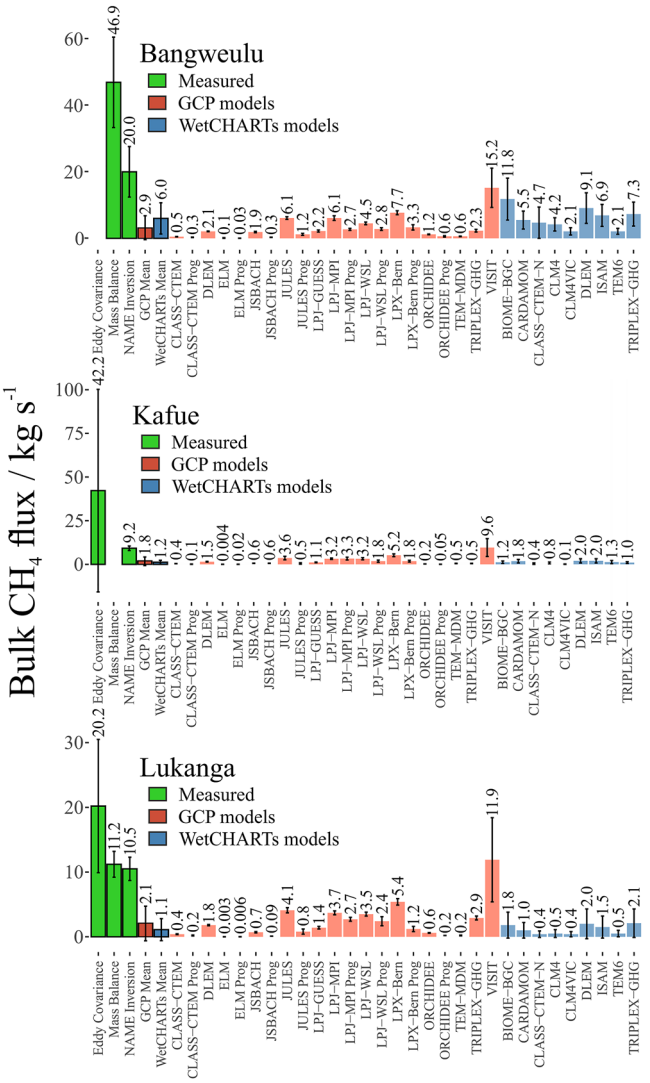

Figure 8. Comparison of measured and land-surface-model simulated bulk Methane (CH_4) fluxes from the three wetlands. Measured emission fluxes for the Bangweulu (top), Kafue (middle), and Lukanga (bottom) wetlands using each of the three flux quantification methods are shown in green. Simulated CH_4 emission fluxes are shown in light red and light blue, for the Global Carbon Project (GCP) and WetCHARTs model suites, respectively, with the means of each of the model ensembles shown in darker shades of the same colors. Error bars show 1 s.d. uncertainty in the case of measurements and 1 s.d. in the distribution of CH_4 emissions across relevant model grid cells in the case of simulations. All models underestimate CH_4 emission fluxes when compared with the measurements. See Supplementary Information Table S5 in Supporting Information S1 for detail.

4. Conclusions

We report the first measurements of CH_4 mole fraction over three large wetland regions in Zambia. Three independent approaches to flux quantification were used to calculate CH_4 emission fluxes. While the quantified emissions were in broad agreement within uncertainties, the use of three different methods demonstrated the advantages and limitations of each of the methods, and their applicability to different sampling regimes and in varying environmental circumstances. The isotopic signature of the wetland CH_4 emissions was measured to be −59.8‰ (±1.0‰). This source signature is lighter than the bulk global background (−47‰) and is consistent with CH_4 emitted from other tropical wetlands (Nisbet et al., 2019). Substantial emissions of such a source would act to drive the global background isotope fraction lighter, consistent with recent trends in the isotopic composition of the global CH_4 budget observed since 2007. The isotopic signature reported here will be useful to better constrain tropical African wetland sources in global CH_4 budget models that use $^{13}C_{CH_4}$ as a co-constraint (Lan et al., 2021). Our results show that the Bangweulu wetland, in the Upper Congo basin, may contribute over 1 Tg CH_4 per year alone, roughly equivalent to half the anthropogenic CH_4 emitted annually by the UK (~50 Tg CO_2 equivalents in 2019; Brown et al., 2021).

While there were differences in the emissions estimated using each of the three flux quantification approaches, it is important to note that all three approaches estimated greater CH_4 emissions than all land surface models. Hence, we provide evidence for the underestimation of wetland CH_4 emissions in the tropics by land surface models (bottom-up) compared with aircraft data (top-down). This finding is consistent with recent global budget assessments (Saunois et al., 2020) which derived bottom-up emission estimates from wetlands of 145 (100–183) Tg CH_4 yr^{-1} but top-down emission estimates of 194 (155–217) Tg CH_4 yr^{-1} for the year 2017. Improvements to land surface models, especially regarding the parameterization of CH_4 emission and the modeling of vegetation typical of tropical wetlands, may be important to better reconcile bottom-up and top-down budgeting approaches.

There is an open question as to how CH_4 emissions from natural wetlands will respond to global climate change (such as increasing surface temperature and tropical rainfall). Such questions cannot be answered within the scope of this study. Further work is urgently needed in tropical Africa, and other regions with vegetated wetlands, to better understand the processes controlling the spatial and temporal distribution of this CH_4 source, and to determine how this source might respond to current and future climate change. If the warming is indeed feeding the warming, this would necessitate imposing additional reduction measures on top of those currently planned for anthropogenic greenhouse gas emissions in order to keep global warming below a threshold of 2°C above preindustrial levels.

Conflict of Interest

The authors declare no conflicts of interest relevant to this study.

Data Availability Statement

Data from the MOYA ZWAMPS aircraft campaign are available from the Centre for Environmental Data Analysis (CEDA) archive (https://www.ceda.ac.uk), at https://catalogue.ceda.ac.uk/uuid/dd2b03d085c5494a8cbfc6b4b99ca702. Please note that access to CEDA data sets and resources requires a free CEDA login account. This is in-line with funder policy and ensures appropriate use and citation of public data. TROPOMI data are available via the online portal at https://ftp.sron.nl/open-access-data-2/TROPOMI/tropomi/ch4/. The latest version of the University of Leicester GOSAT Proxy v9.0 XCH4 data are available from the CEDA archive at https://doi.org/10.5285/18ef8247f52a4cb6a14013f8235cc1eb. The GOSAT data used in this study are also available from the Copernicus C3S Climate Data Store at https://cds.climate.copernicus.eu. Data sets contributing to the Global Carbon Project 2020 Global Methane Budget are archived in ICOS at https://doi.org/10.5194/essd-12-1561-2020. The WetCHARTs ensembles are available from the Oak Ridge National Laboratory Distributed Active Archive Center (ORNL DAAC; http://dx.doi.org/10.3334/ORNLDAAC/1502). The GEOS-Chem model code is available at http://acmg.seas.harvard.edu/geos. The eddy4R v.0.2.0 software framework used to generate eddy-covariance flux estimates can be freely accessed at https://github.com/NEONScience/eddy4R. The eddy4R turbulence v0.0.16 software model for advanced airborne data processing was accessed under Terms of Use for this study (https://www.eol.ucar.edu/content/cheesehead-code-policy-appendix) and is available upon request.

Acknowledgments
The aircraft data used in this publication have been collected as part of the Methane Observations and Yearly Assessments (MOYA) project funded by the Natural Environment Research Council (NERC) under Grant No. NE/N015835/1 (The University of Manchester) and NE/N016211/1 (Royal Holloway, University of London), as well as the NERC ZWAMPS project (NE/S00159X/1). MFL and PIP also acknowledge funding from MOYA (NE/N015916/1) and the NERC National Centre for Earth Observation (NE/R016518/1). AG is funded by a NERC Independent Research Fellowship (NE/L010992/1). RJP is funded via the UK National Centre for Earth Observation (NE/N018079/1 and NE/R016518/1). NG acknowledges funding from MOYA and from The Newton Fund via the Met Office Climate Science for Service Partnership Brazil (CSSP Brazil). SM acknowledges the National Ecological Observatory Network (NEON), a program sponsored by the National Science Foundation and operated under cooperative agreement by Battelle. This material is based in part upon work supported by the National Science Foundation through the NEON Program. We would like to thank Airtask Ltd. (who flew the aircraft),and all those involved in the operation and maintenance of the BAe-146-301 Atmospheric Research Aircraft including FAAM, Avalon Aero, UK Research and Innovation (UKRI) and the University of Leeds. We also thank The Zambian Geological Survey, Ministry of Mines, Zambia for their very strong support and participation in all stages of the work in Zambia. We would like to thank the Japanese Aerospace Exploration Agency, National Institute for Environmental Studies, and the Ministry of Environment for the GOSAT data and their continuous support as part of the Joint Research Agreement. This research used the ALICE High Performance Computing Facility at the University of Leicester for the GOSAT retrievals. GCP land surface model work contributions: CTEM, Joe Melton, Vivek Arora; DLEM, Hanqin Tian, Hao Shi; ELM, William Riley, Qing Zhu; JSBACH, Thomas Kleinen; JULES, Nicola Gedney; LPJ-GUESS, Paul Miller, Wenxin Zhang; LPJ-MPI, Thomas Kleinen; LPJ-wsl, Ben Poulter, Zhen Zhang; LPX-Bern, Jurek Muller, Fortunat Joos; ORCHIDEE, Sushi Peng; TEM-MDM, Qianlai Zhuang, Licheng Liu; TRIPLEX-GHG, Changhui Peng, Qiuan Zhu; VISIT, Akihiko Ito.Any opinions, findings, conclusions or recommendations expressed in this material are those of the author(s) and do not necessarily reflect the views of their respective institutions.

References

Barba, J., Bradford, M. A., Brewer, P. E., Bruhn, D., Covey, K., van Haren, J., et al. (2018). Methane emissions from tree stems: A new Frontier in the global carbon cycle. *New Phytologist*, *222*, 18–28. https://doi.org/10.1111/nph.15582

Barker, P. A., Allen, G., Gallagher, M., Pitt, J. R., Fisher, R. E., Bannan, T., et al. (2020). Airborne measurements of fire emission factors for African biomass burning sampled during the MOYA campaign. *Atmospheric Chemistry and Physics*, *20*, 15443–15459. https://doi.org/10.5194/acp-20-15443-2020

Billesbach, D. P. (2011). Estimating uncertainties in individual eddy covariance flux measurements: A comparison of methods and a proposed new method. *Agricultural and Forest Meteorology*, *151*, 394–405. https://doi.org/10.1016/j.agrformet.2010.12.001

Bloom, A. A., Bowman, K. W., Lee, M., Turner, A. J., Schroeder, R., Worden, J. R., et al. (2017). A global wetland methane emissions and uncertainty dataset for atmospheric chemical transport models (WetCHARTs version 1.0). *Geoscientific Model Development*, *10*, 2141–2156. https://doi.org/10.5194/gmd-10-2141-2017

Blyth, E. M., Arora, V. K., Clark, D. B., Dadson, S. J., De Kauwe, M. G., Lawrence, D. M., et al. (2021). Advances in land surface modelling. *Current Climate Change Reports*, *7*, 45–71. https://doi.org/10.1007/s40641-021-00171-5

Bontemps, S., Defourny, P., Bogaert, E. V., Arino, O., Kalogirou, V., & Perez, J. R. (2011). GlobCover products description and validation report. *Tech. rep. ESA*.

Brioude, J., Angevine, W. M., Ahmadov, R., Kim, S.-W., Evan, S., McKeen, S. A., et al. (2013). Top-down estimate of surface flux in the Los Angeles Basin using a mesoscale inverse modelling technique: Assessing anthropogenic emissions of CO, NO_x and CO_2 and their impacts. *Atmospheric Chemistry and Physics*, *13*, 3661–3677. https://doi.org/10.5194/acp-13-3661-2013

Brown, P., Cardenas, L., Choudrie, S., Del Vento, S., & Karagianni, E. (2021). *UK greenhouse gas inventory, 1990 to 2019: Annual report for submission under the framework convention on climate change*, Department for Business, Energy & Industrial Strategy, Ricardo Energy & Environment, 978-0-9933975-7-8.

Butz, A., Guerlet, S., Hasekamp, O., Schepers, D., Galli, A., Aben, C., et al. (2011). Toward accurate CO_2 and CH_4 observations from GOSAT. *Gephysical Research Letter*, *38*, L14812. https://doi.org/10.1029/2011gl047888

Cambaliza, M. O., Shepson, P. B., Caulton, D. R., Stirm, B., Samarov, D., Gurney, K. R., et al. (2014). Assessment of uncertainties of an aircraft-based mass balance approach for quantifying urban greenhouse gas emissions. *Atmospheric Chemistry and Physics*, *14*, 9029–9050. https://doi.org/10.5194/acp-14-9029-2014

Comyn-Platt, E., Hayman, G., Huntingford, C., Chadburn, S. E., Burke, E. J., Harper, A. B., et al. (2018). Carbon budgets for 1.5 and 2°C targets lowered by natural wetland and permafrost feedbacks. *Nature Geoscience*, *11*, 568–573. https://doi.org/10.1038/s41561-018-0174-9

Dalmagro, H. J., de Zanella, Arruda, P. H., Vourlitis, G. L., Lathuillière, M. J., Nogueria, J. de. S., Couto, E. G., & Johnson, M. S. (2019). Radiative forcing of methane fluxes offsets net carbon dioxide uptake for a tropical flooded forest. *Global Change Biology*, *25*, 1967–1981. https://doi.org/10.1111/gcb.14615

Daly, M. C., Green, P., Watts, A. B., Davies, O., Chibesakunda, F., & Walker, R. (2020). Tectonics and landscape of the Central African Plateau and their implications for a propagating Southwestern rift in Africa. *Geochemistry, Geophysics, Geosystems*, *21*, e2019GC008746. https://doi.org/10.1029/2019gc008746

Dean, J. F., Middelburg, J. J., Röckmann, T., Aerts, R., Blauw, L., Egger, M., et al. (2018). Methane feedbacks to the global climate system in a warmer world. *Review of Geophysics*, *56*, 207–250. https://doi.org/10.1002/2017rg000559

Deardorff, J. W. (1974). Three-dimensional numerical study of turbulence in an entraining mixed layer. *Boundary-Layer Meteorology*, *7*, 199–226. https://doi.org/10.1007/bf00227913

Debenham, F. (1952). *Study of an African swamp: The Bangweulu Swamps, northern Rhodesia, published for the government of northern Rhodesia by H.M.S.O*.

Dee, D. P., Uppala, S. M., Simmons, A. J., Berrisford, P., Poli, P., Kobayashi, S., et al. (2011). The ERA-Interim reanalysis: Configuration and performance of the data assimilation system. *Quarterly Journal of the Royal Meteorological Society*, *137*, 656. https://doi.org/10.1002/qj.828

Denmead, O. T., Leuning, R., Griffith, D. W. T., & Meyer, C. P. (1999). Some recent developments in trace gas flux measurement techniques. *Developments in Atmospheric Science*, *24*, 69–84. https://doi.org/10.1016/s0167-5117(98)80024-4

Denmead, O. T., Raupach, M. R., Dunin, F. X., Cleugh, H. A., & Leuning, R. (1996). Boundary layer budgets for regional estimates of scalar fluxes. *Global Change Biology*, *2*, 3. https://doi.org/10.1111/j.1365-2486.1996.tb00077.x

Dlugokencky, E. *NOAA/ESRL*. Retrieved from www.esrl.noaa.gov/gmd/ccgg/trends_ch4

Fiehn, A., Kostinek, J., Eckl, M., Klausner, T., Gałkowski, M., Chen, J., et al. (2020). Estimating CH_4, CO_2 and CO emissions from coal mining and industrial activities in the Upper Silesian Coal Basin using an aircraft-based mass balance approach. *Atmospheric Chemistry and Physics*, *20*, 12675–12695. https://doi.org/10.5194/acp-20-12675-2020

Fisher, R., Lowry, D., Wilkin, O., Sriskantharajah, S., & Nisbet, E. G. (2006). High-precision, automated stable isotope analysis of atmospheric methane and carbon dioxide using continuous-flow isotope-ratio mass spectrometry. *Rapid Communications in Mass Spectrometry*, *20*, 200–208. https://doi.org/10.1002/rcm.2300

Fisher, R. E., France, J. L., Lowry, D., Lanoisellé, M., Brownlow, R., Pyle, J. A., et al. (2017). Measurement of the ^{13}C isotopic signature of methane emissions from northern European wetlands. *Global Biogeochemical Cycles*, *31*, 605–623. https://doi.org/10.1002/2016gb005504

Foken, T., & Wichura, B. (1996). Tools for quality assessment of surface-based flux measurements. *Agricultural and Forest Meteorology*, *78*, 83–105. https://doi.org/10.1016/0168-1923(95)02248-1

Ganesan, A. L., Rigby, M., Lunt, M. F., Parker, R. J., Boesch, H., Goulding, N., et al. (2017). Atmospheric observations show accurate reporting and little growth in India's methane emissions. *Nature Communications*, *8*, 836. https://doi.org/10.1038/s41467-017-00994-7

Ganesan, A. L., Rigby, M., Zammit-Mangion, A., Manning, A. J., Prinn, R. G., Fraser, P. J., et al. (2014). Characterization of uncertainties in atmospheric trace gas inversions using hierarchical Bayesian methods. *Atmospheric Chemistry and Physics*, *14*, 3855–3864. https://doi.org/10.5194/acp-14-3855-2014

Ganesan, A. L., Schwietzke, S., Poulter, B., Arnold, T., Lan, X., Rigby, M., et al. (2019). Advancing scientific understanding of the global methane budget in support of the Paris Agreement. *Global Biogeochem Cycles*, *33*, 1475–1512. https://doi.org/10.1029/2018GB006065

Ganesan, A. L., Stell, A. C., Gedney, N., Comyn-Platt, E., Hayman, G., Rigby, M., et al. (2018). Spatially resolved isotopic source signatures of wetland methane emissions. *Geophysical Research Letters*, *45*, 3737–3745. https://doi.org/10.1002/2018gl077536

Gumbricht, T., Román-Cuesta, R. M., Verchot, L. V., Herold, M., Wittmann, F., Householder, E., et al. (2017b). An expert system model for mapping tropical wetlands and peatlands reveals South America as the largest contributor. *Global Change Biology*, *23*, 3581–3599. https://doi.org/10.1111/gcb.13689

Gumbricht, T., Román-Cuesta, R. M., Verchot, L. V., Herold, M., Wittmann, F., Householder, E., et al. (2017a). Tropical and Subtropical Wetlands Distribution Version 2, Center for International Forestry Research, V3, UNF:6:Bc9aFtBpam27aFOCMgW71Q. https://doi.org/10.17528/CIFOR/DATA.00058

Hannun, R. A., Wolfe, G. M., Kawa, S. R., Hanisco, T. F., Newman, P. A., Alfieri, J. G., et al. (2020). Spatial heterogeneity in CO_2, CH_4, and energy fluxes: Insights from airborne eddy covariance measurements over the Mid-Atlanatic region. *Environmental Research Letters*, *15*, 035008. https://doi.org/10.1088/1748-9326/ab7391

Helfter, C., Gondwe, M., Murray-Hudson, M., Makati, A., Lunt, M. F., Palmer, P. I., & Skiba, U. (2022). Phenology is the dominant control of methane emissions in a tropical non-forested wetland. *Nature communications*, *13*, 133. https://doi.org/10.1038/s41467-021-27786-4

Helfter, C., Gondwe, M., Murray-Hudson, M., Makati, A. & Skiba, U. (2021). From sink to source: High inter-annual variability in the carbon budget of a Southern African wetland. *Philosophical Transactions of the Royal Society A*, *380*, 20210148. https://doi.org/10.1098/rsta.2021.0148

Howarth, R. W. (2019). Ideas and perspectives: Is shale gas a major driver of recent increase in global atmospheric methane? *Biogeosciences*, *16*, 3033–3046. https://doi.org/10.5194/bg-16-3033-2019

Hu, H., Hasekamp, O., Butz, A., Galli, A., Landgraf, J., Aan de Brugh, J., et al. (2016). The operational methane retrieval algorithm for TROPOMI. *Atmospheric Measurement Techniques*, *9*, 5423–5440. https://doi.org/10.5194/amt-9-5423-2016

Hughes, R. H., & Hughes, J. S. (1992). *A directory of African wetlands*, IUCN, Gland and Cambridge/UNEP, Nairobi/WCMC.

Information Sheet on Ramsar Wetlands (RIS). (2005). Site number 1580, Lukanga Swamps. Retrieved from https://rsis.ramsar.org/RISapp/files/RISrep/ZM1580RIS.pdf

Information Sheet on Ramsar Wetlands (RIS). (2007a). Site number 530, Kafue Flats. Retrieved from https://rsis.ramsar.org/RISapp/files/RISrep/ZM530RIS.pdf

Information Sheet on Ramsar Wetlands (RIS). (2007b). Site number 531, Bangweulu Swamps. Retrieved from https://rsis.ramsar.org/RISapp/files/RISrep/ZM531RIS.pdf

Jackson, R. B., Saunois, M., Bousquet, P., Canadell, J. G., Poulter, B., Stavert, A. R., et al. (2020). Increasing anthropogenic methane emissions arise equally from agricultural and fossil fuel sources. *Environmental Research Letters*, *15*, 071002. https://doi.org/10.1088/1748-9326/ab9ed2

Janssens-Maenhout, G., Crippa, M., Guizzardi, D., Muntean, M., Schaaf, E., Dentener, F., et al. (2019). EDGAR v4.3.2 global Atlas of the three major greenhouse gas emissions for the period 1970–2012. *Earth System Science Data*, *11*, 959–1002. https://doi.org/10.5194/essd-11-959-2019

Jones, A., Thomson, D., Hort, M., & Devenish, B. (2007). *The UK met office's next-generation atmospheric dispersion model*, NAME III. 580–589. https://doi.org/10.1007/978-0-387-68854-1_62

Kaiser, J. W., Heil, A., Andrae, M. I., Benedetti, A., Chubarova, N., Jones, L., et al. (2012). Biomass burning emissions estimated with a global fire assimilation system based on observed fire radiative power. *Biogeosciences*, *9*, 527–554. https://doi.org/10.5194/bg-9-527-2012

Kim, D.-G., Thomas, A. D., Pelster, D., Rosenstock, T. S., & Sanz-Cobena, A. (2016). Greenhouse gas emissions from natural ecosystems and agricultural lands in sub-Saharan Africa: A synthesis of available data and suggestions for future research. *Biogeosciences*, *13*, 4789–4809. https://doi.org/10.5194/bg-13-4789-2016

Kuze, A., Suto, H., Nakajima, M., & Hamazaki, T. (2009). Thermal and near infrared sensor for carbon observation Fourier-transform spectrometer on the Greenhouse Gases Observing Satellite for greenhouse gases monitoring. *Applied Optics*, *48*, 6716–6733. https://doi.org/10.1364/ao.48.006716

Lan, X., Nisbet, E. G., Dlugokencky, E. J., & Michel, S. E. (2021). What do we know about the global methane budget? Results from four decades of atmospheric CH_4 observations and the way forward. *Philosophical Transactions of the Royal Society A*, *379*, 20200440. https://doi.org/10.1098/rsta.2020.0440

Lehner, B., & Döll, P. (2004). Development and validation of a global database of lakes, reservoirs and wetlands. *Journal of Hydrology*, *296*, 1–22. https://doi.org/10.1016/j.jhydrol.2004.03.028

Lenschow, D. H., Mann, J., & Kristensen, L. (1994). How long is long enough when measuring fluxes and other turbulent statistics? *Journal of Atmosphere Ocean Technology*, *11*, 661–673. https://doi.org/10.1175/1520-0426(1994)011<0661:hlilew>2.0.co;2

Lopez-Coto, I., Ren, X., Salmon, O. E., Karion, A., Shepson, P. B., Dickerson, R. R., et al. (2020). Wintertime CO_2, CH_4 and CO emissions estimation for the Washington, DC-Baltimore Metropolitan area using an inverse modelling technique. *Environmental Science Technology*, *54*, 2606–2614. https://doi.org/10.1021/acs.est.9b06619

Lorente, A., Borsdorff, T., Butz, A., Hasekamp, O., aan de Brugh, J., Schneider, A., et al. (2021). Methane retrieved from TROPOMI: Improvement of the data product and validation of the first two years of measurements. *Atmospheric Measurement Techniques*, *14*, 665–684. https://doi.org/10.5194/amt-14-665-2021

Lunt, M. F., Palmer, P. I., Feng, L., Taylor, C. M., Boesch, H., & Parker, R. J. (2019). An increase in methane emissions from tropical Africa between 2010 and 2016 inferred from satellite data. *Atmospheric Chemistry and Physics*, *19*, 14721–14740. https://doi.org/10.5194/acp-19-14721-2019

Lunt, M. F., Palmer, P. I., Lorente, A., Borsdorff, T., Landgraf, J., Parker, R. J., & Boesch, H. (2021). Rain-fed pulses of methane from East Africa during 2018–2019 contributed to atmospheric growth rate. *Environmental Research Letters*, *16*, 024021. https://doi.org/10.1088/1748-9326/abd8fa

Mann, J., & Lenschow, D. H. (1994). Errors in airborne flux measurements. *Journal of Geophysical Research: Atmospheres*, *99*, 14519–14526. https://doi.org/10.1029/94jd00737

Marani, L., & Alvalá, P. C. (2007). Methane emissions from lakes and floodplains in Pantanal, Brazil. *Atmospheric Environment*, *41*, 1627–1633. https://doi.org/10.1016/j.atmosenv.2006.10.046

McNorton, J., Wilson, C., Gloor, M., Parker, R. J., Boesch, H., Feng, W., et al. (2018). Attribution of recent increases in atmospheric methane through 3-D inverse modelling. *Atmospheric Chemistry and Physics*, *18*, 18149–18168. https://doi.org/10.5194/acp-18-18149-2018

Melton, J. R., Wania, R., Hodson, E. L., Poulter, B., Ringeval, B., Spahni, R., et al. (2013). Present state of global wetland extent and wetland methane modelling: Conclusions from a model intercomparison project (WETCHIMP). *Biogeosciences*, *10*, 753–788. https://doi.org/10.5194/bg-10-753-2013

Metzger, S., Durden, D., Sturtevant, C., Luo, H., Pingintha-Durden, N., Sachs, T., et al. (2017). eddy4R 0.2.0: A DevOps model for community-extensible processing and analysis of eddy-covariance data based on R, Git, Docker, and HDF5. *Geoscientific Model Development*, *10*, 3189–3206. https://doi.org/10.5194/gmd-10-3189-2017

Metzger, S., Junkermann, W., Mauder, M., Beyrich, F., Butterbach-Bahl, K., Schmid, H. P., & Foken, T. (2012). Eddy-covariance flux measurements with a weight-shift microlight aircraft. *Atmospheric Measurement Techniques*, *5*, 1699–1717. https://doi.org/10.5194/amt-5-1699-2012

Metzger, S., Junkermann, W., Mauder, M., Butterbach-Bahl, K., Widemann, B. T. Y., Neidl, F., et al. (2013). Spatially explicit regionalization of airborne flux measurements using environmental response functions. *Biogeosciences*, *10*, 2193–2217. https://doi.org/10.5194/bg-10-2193-2013

Milkov, A. V., Schwietzke, S., Allen, G., Sherwood, O. A., & Etiope, G. (2020). Using global isotopic data to constrain the role of shale gas production in recent increases in atmospheric methane. *Scientific Reports*, *10*, 4199. https://doi.org/10.1038/s41598-020-61035-w

Miller, J. B., & Tans, P. P. (2003). Calculating isotopic fractionation from atmospheric measurements at various scales. *Tellus B: Chemical and Physical Meteorology*, *55*, 207–214. https://doi.org/10.1034/j.1600-0889.2003.00020.x

Nahlik, A. M., & Mitsch, W. J. (2011). Methane emissions from tropical freshwater wetlands located in different climatic zones of Costa Rica. *Global Change Biology*, *17*, 1321–1334. https://doi.org/10.1111/j.1365-2486.2010.02190.x

Nisbet, E. G., Dlugokencky, E. J., Manning, M. R., Lowry, D., Fisher, R. E., France, J. L., et al. (2016). Rising atmospheric methane: 2007–2014 growth and isotopic shift. *Global Biogeochemical Cycles*, *30*, 1356–1370. https://doi.org/10.1002/2016gb005406

Nisbet, E. G., Manning, M. R., Dlugokencky, E. J., Fisher, R. E., Lowry, D., Michel, S. E., et al. (2019). Very strong atmospheric methane growth in the 4 years 2014-2017: Implications for the Paris Agreement. *Global Biogeochemical Cycles*, *33*, 318–342. https://doi.org/10.1029/2018gb006009

O'Shea, S. J., Allen, G., Gallagher, M. W., Bower, K., Illingworth, S. M., Muller, J. B. A., et al. (2014). Methane and carbon dioxide fluxes and their regional scalability for the European Arctic wetlands during the MAMM project in summer 2012. *Atmospheric Chemistry and Physics*, *14*, 13159–13174. https://doi.org/10.5194/acp-14-13159-2014

O'Shea, S. J., Bauguitte, S. J.-B., Gallagher, M. W., Lowry, D., & Percival, C. J. (2013). Development of a cavity-enhanced absorption spectrometer for airborne measurements of CH_4 and CO_2. *Atmospheric Measurement Techniques*, *6*, 1095–1109. https://doi.org/10.5194/amt-6-1095-2013

Palmer, P. I., Feng, L., Lunt, M. F., Parker, R. J., Bösch, H., Lan, L., et al. (2021). The added value of satellite observations for understanding the contemporary methane budget. *Philosophical Transactions of the Royal Society A*, *379*, 20210106. https://doi.org/10.1098/rsta.2021.0106

Pandey, S., Houweling, S., Lorente, A., Borsdorff, T., Tsivludou, M., Bloom, A. A., et al. (2021). Using satellite data to identify the methane emission controls of South Sudan's wetlands. *Biogeosciences*, *18*, 557–572. https://doi.org/10.5194/bg-18-557-2021

Pangala, S. R., Enrich-Prast, A., Basso, L. S., Peixoto, R. B., Bastviken, D., Hornibrook, E. R. C., et al. (2017). Large emissions from floodplain trees close the Amazon methane budget. *Nature*, *552*, 230–234. https://doi.org/10.1038/nature24639

Parker, R. J., Boesch, H., McNorton, J., Comyn-Platt, E., Gloor, M., Wilson, C., et al. (2018). Evaluating year-to-year anomalies in tropical wetland methane emissions using satellite CH_4 observations. *Remote Sensing of Environment*, *211*, 261–275. https://doi.org/10.1016/j.rse.2018.02.011

Parker, R. J., Webb, A., Boesch, H., Somkuti, P., Guillo, R. B., Di Noia, A., et al. (2020). A decade of GOSAT Proxy satellite CH_4 observations. *Earth System Science Data*, *12*, 3383–3412. https://doi.org/10.5194/essd-12-3383-2020

Parker, R. J., Wilson, C., Bloom, A. A., Comyn-Platt, E., Hayman, G., McNorton, J., et al. (2020). Exploring constrants on a wetland methane emission ensemble (WetCHARTs) using GOSAT observations. *Biogeosciences*, *17*, 5669–5691. https://doi.org/10.5194/bg-17-5669-2020

Pisso, I., Patra, P., Takigawa, M., Machida, T., Matsueda, H., & Sawa, Y. (2019). Assessing Lagrangian inverse modelling of urban anthropogenic CO_2 fluxes using in situ aircraft and ground-based measurements in the Tokyo area. *Carbon Balance Manage*, *14*, 6. https://doi.org/10.1186/s13021-019-0118-8

Pitt, J. R., Allen, G., Bauguitte, S. J.-B., Gallagher, M. W., Lee, J. D., Drysdale, W., et al. (2019). Assessing London CO_2, CH_4, and CO emissions using aircraft measurements and dispersion modelling. *Atmospheric Chemistry and Physics*, *19*, 8931–8945. https://doi.org/10.5194/acp-19-8931-2019

Rigby, M., Montzka, S. A., Prinn, R. G., White, J. W. C., Young, D., O'Doherty, S., et al. (2017). Role of atmospheric oxidation in recent methane growth. *Proceedings of the National Academy of Sciences of the United States of America*, *114*, 5373–5377. https://doi.org/10.1073/pnas.1616426114

Rigby, M., Park, S., Saito, T., Western, L. M., Redington, A. L., Fang, X., et al. (2019). Increase in CFC-11 emissions from eastern China based on atmospheric observations. *Nature*, *569*, 546–550. https://doi.org/10.1038/s41586-019-1193-4

Saunois, M., Stavert, A. R., Poulter, B., Bousquet, P., Canadell, J. G., Jackson, R. B., et al. (2020). The global methane budget 2000–2017. *Earth System Science Data*, *12*, 1561–1623. https://doi.org/10.5194/essd-12-1561-2020

Say, D., Kuyper, B., Western, L., Anwar, M., Khan, H., Lesch, T., et al. (2020). Emissions and marine boundary layer concentrations of unregulated chlorocarbons measured at Cape Point, South Africa. *Environmental Science & Technology*, *54*, 10514–10523. https://doi.org/10.1021/acs.est.0c02057

Schaefer, H., Mikaloff-Fletcher, S. E., Veidt, C., Lassey, K. R., Brailsford, G. W., Bromley, T. M., et al. (2016). A 21st century shift from fossil fuel to biogenic methane emissions indicated by $^{13}CH_4$. *Science*, *352*, 80–84. https://doi.org/10.1126/science.aad2705

Schroeder, R., McDonald, K. C., Chapman, B. D., Jensen, K., Podest, E., Tessler, Z. D., et al. (2015). Development and evaluation of a multi-year fractional surface water data set derived from active/passive microwave remote sensing data. *Remote Sensing*, *7*, 16688–16732. https://doi.org/10.3390/rs71215843

Schwieztke, S., Sherwood, O. A., Bruhwiler, L. M. P., Miller, J. B., Etiope, G., Dlugokencky, E. J. et al. (2016). Upward revision of global fossil fuel methane emissions based on isotope database. *Nature*, *538*, 88–91. https://doi.org/10.1038/nature19797

Smith, P. (2001). *Ecological survey of Zambia*. Published by Royal Botanical Gardens, pp. 1404. ISBN-13: 978-1-84246-005-4.

Sorbjan, Z. (2006). Statistics of scalar fields in the atmospheric boundary layer based on large-eddy simulations. Part II: Forced convection. *Boundary-Layer Meteorology*, *119*, 57–79. https://doi.org/10.1007/s10546-005-9014-8

Travaglia, C., & Macintosh, H. (1997). *Wetlands monitoring by ERS-SAR data; A case study; Lake Bangweulu wetland system, Zambia*, *RSC Series*, (Vol. 69), Food and Agriculture Organisation of the United Nations.

Tunnicliffe, R. L., Ganesan, A. L., Parker, R. J., Boesch, H., Gedney, N., Poulter, B., et al. (2020). Quantifying sources of Brazil's CH_4 emissions between 2010 and 2018 from satellite data. *Atmospheric Chemistry and Physics*, *20*, 13041–13067. https://doi.org/10.5194/acp-20-13041-2020

Turner, A. J., Jacob, D. J., Wecht, K. J., Maasakkers, J. D., Lundgren, E., Andrews, A. E., et al. (2015). Estimating global and North American methane emissions with high spatial resolution using GOSAT satellite data. *Atmospheric Chemistry and Physics*, *15*, 7049–7069. https://doi.org/10.5194/acp-15-7049-2015

van der Werf, G. R., Randerson, J. T., Giglio, L., van Leeuwen, T. T., Chen, Y., Rogers, B. M., et al. (2017). Global fire emissions estimates during 1997–2016. *Earth System Science Data*, *9*, 697–720. https://doi.org/10.5194/essd-9-697-2017

Vaughan, A. R., Lee, J. D., Metzger, S., Durden, D., Lewis, A. C., Shaw, M. D., et al. (2021). Spatially and temporally resolved measurements of NO_x fluxes by airborne eddy covariance over Greater London. *Atmospheric Chemistry and Physics*, *21*, 15283–15298. https://doi.org/10.5194/acp-21-15283-2021

Vaughan, A. R., Lee, J. D., Misztal, P. K., Metzger, S., Shaw, M. D., Lewis, A. C., et al. (2016). Spatially resolved flux measurements of NO_x from London suggest significantly higher emissions than predicted by inventories. *Faraday Discussions*, *189*, 455–472. https://doi.org/10.1039/c5fd00170f

Vickers, D., & Mahrt, L. (1997). Quality control and flux sampling problems for tower and aircraft data. *Journal of Atmospheric and Oceanic Technology*, *14*, 512–526. https://doi.org/10.1175/1520-0426(1997)014<0512:qcafsp>2.0.co;2

Wecht, K. J., Jacob, D. J., Frankenburg, C., Jiang, Z., & Blake, D. R. (2014). Mapping of North American methane emissions with high spatial resolution by inversion of SCIAMACHY satellite data. *Journal of Geophysical Research: Atmospheres*, *119*, 7741–7756. https://doi.org/10.1002/2014jd021551

Wilson, C., Chipperfield, M. P., Gloor, M., Parker, R. J., Boesch, H., McNorton, J., et al. (2021). Large and increasing methane emissions from eastern Amazonia derived from satellite data, 2010–2018. *Atmospheric Chemistry and Physics*, *21*, 10643–10669. https://doi.org/10.5194/acp-21-10643-2021

Wu, H., Taylor, J. W., Langridge, J. M., Yu, C., Allan, J. D., Szpek, K., et al. (2021). Rapid transformation of ambient absorbing aerosols from West African biomass burning. *Atmospheric Chemistry and Physics*, *21*, 9417–9440. https://doi.org/10.5194/acp-21-9417-2021

Xu, X., Yuan, F., Hanson, P. J., Wullschleger, S. D., Thornton, P. E., Riley, W. J., et al. (2016). Reviews and syntheses: Four decades of modelling methane cycling in terrestrial ecosystems. *Biogeosciences*, *13*, 3735–3755. https://doi.org/10.5194/bg-13-3735-2016

Zhang, Z., Fluet-Chouinard, E., Jensen, K., McDonald, K., Hugelius, G., Gumbricht, T., et al. (2021). Development of the global dataset of wetland area and dynamics for methane modeling (WAD2M). *Earth System Science Data*, *13*, 2001–2023. https://doi.org/10.5194/essd-13-2001-2021

References From the Supporting Information

Buchhorn, M., Smets, B., Bertels, L., de Roo, B., Lesiv, M., Tsendbazar, N.-E., et al. (2020). *Copernicus global land Service: Land cover 100m: Collection 3: Epoch 2019*, Globe. https://doi.org/10.5281/zenodo.3939050

Gray, W. (2007). Zambia and Victoria Falls. New Holland Publishers. P91. 9781845378134.

McCartney, M., Rebelo, L.-M., Mapedza, E., de Silva, S., & Finlayson, C. M. (2011). The Lukanga Swamps: Use, conflicts and management. *Journal of International Wildlife Law and Policy*, *14*, 293–310. https://doi.org/10.1080/13880292.2011.626720

van den Bossche., & Bernacsek. (1990). Source Book for the Inland Fishery Resources of Africa, 1.